# Enhanced Light Absorption and Elevated Viscosity of Atmospheric Brown Carbon through Evaporation of Volatile Components

Diego Calderon-Arrieta<sup>a</sup>, Ana C. Morales<sup>a</sup>, Anusha Priyadarshani Silva Hettiyadura<sup>a</sup>, Taylor M. Estock<sup>a</sup>, Chunlin Li<sup>c,†</sup>, Yinon Rudich<sup>c</sup>, and Alexander Laskin\*<sup>a,b</sup>

<sup>a</sup> Department of Chemistry, <sup>b</sup> Department of Earth, Atmospheric and Planetary Sciences, Purdue University, West Lafayette, IN, 47907, USA

<sup>c</sup> Department of Earth and Planetary Sciences, Weizmann Institute of Science, Rehovot 76100, Israel

<sup>†</sup> present address College of Environmental Science and Engineering, Tongji University, Shanghai 200072, China

\* phone: (765) 494-5243; email: alaskin@purdue.edu

**KEYWORDS:** gas-particle partitioning, aerosol chemistry, aerosol volatility, aerosol viscosity, molecular composition, high performance liquid chromatography, high-resolution mass spectrometry

Manuscript submitted to

Environmental Science and Technology

March 27, 2024

ABSTRACT: Samples of Brown carbon (BrC) material were collected from smoke emissions originating from wood pyrolysis experiments, serving as a proxy for BrC representative of biomass burning emissions. The acquired samples, referred to as "pyrolysis oil (PO<sub>1</sub>)," underwent subsequent processing by thermal evaporation of their volatile compounds, resulting in a set of three additional samples with the volume reduction factors of 1.25, 2, and 3, denoted as PO<sub>1.25</sub>, PO<sub>2</sub>, and PO<sub>3</sub>. The chemical composition of these PO<sub>x</sub> samples and their BrC chromophore features were analyzed using a high performance liquid chromatography instrument coupled with a photodiode array detector and a high-resolution mass spectrometer. The investigation revealed a noteworthy twofold enhancement of BrC light absorption observed for the progression of PO<sub>1</sub> to PO<sub>3</sub> samples, assessed across the spectral range of 300-500 nm. Concurrently, a decrease in the absorption Ångstrom exponent (AAE) from 11 to 7 was observed, indicating a weaker spectral dependence. The relative enhancement of BrC absorption at longer wavelengths was more significant, as exemplified by the increased mass absorption coefficients (MAC) measured at 405 nm from 0.1 to 0.5 m<sup>2</sup>/g. Molecular characterization further supports this darkening trend, manifesting as a depletion of small oxygenated, less absorbing monoaromatic compounds and the retention of relatively large, less polar, more absorbing constituents. Noteworthy alterations of the PO<sub>1</sub> to PO<sub>3</sub> mixtures included a reduction of the saturation vapor pressure of their components and an increase in viscosity. These changes were quantified by mean values shifting from approximately  $1.8 \times 10^3$  µg/m<sup>3</sup> to 2.3 µg/m<sup>3</sup> and from  $\sim 10^3$  Pa·s to  $\sim 10^6$  Pa·s, respectively. These results provide quantitative insights into the extent of BrC aerosol darkening during atmospheric aging through non-reactive evaporation. This newfound understanding will inform the refinement of atmospheric and chemical transport models.

#### **SYNOPSIS**

Non-reactive evaporation of BrC compounds facilitates degassing of weakly-absorbing small monoaromatic species and an enrichment of strongly-absorbing larger lignin decomposition products and substituted polycyclic aromatic hydrocarbons (PAHs).

## 1. INTRODUCTION

Accurate prediction of the atmospheric environment and radiative forcing of the climate requires an improved understanding of the composition and optical properties of biomass burning aerosols, which contain a significant amount of light-absorbing organic components termed brown carbon (BrC).<sup>1-4</sup> As the frequency and intensity of wildfires increase as a result of a warmer and drier climate, BrC becomes a profound contributor to the overall radiative forcing.<sup>5-7</sup> This is attributed to its capacity to absorb solar radiation within the UV and visible wavelengths.<sup>5,8-15</sup> Additionally, the widespread use of biomass fuels and practices of agricultural burning in developing countries amplifies BrC emissions and its significance.<sup>16-19</sup> The upsurge in BrC aerosols from biomass burning (BB) disturbs various climate and atmospheric processes, including long range transport of atmospheric pollutants, cloud condensation and ice nucleation, alterations in snow and ice albedo, and reduced photodegradation rates.<sup>20-26</sup> The extent to which BB-BrC aerosols influence these processes remains uncertain, which makes it challenging for atmospheric models to accurately project their global impact, both presently and in the future.

BrC exhibits a broad range of optical properties due to its diverse sources and dynamic transformations during atmospheric aging.<sup>27–32</sup> Recent studies have begun revealing the relationship between BrC's optical properties and its chemical composition.<sup>33–58</sup> Accordingly, BrC is classified into four optically-based groups: very-weakly (VW), weakly (W), moderately (M), or

strongly (S) – absorbing BrC.<sup>59</sup> The VW group portrays BrC formed in secondary organic aerosol, while the W and M groups represent BrC originating from primary BB emissions. 60-64 The S group delineates highly viscous particles that have undergone significant transformations, such as refractory carbonaceous spheres (tar balls).65,66 Chemical analysis of BrC materials representing these groups has revealed distinct physicochemical properties, including unique wavelength absorption spectra, molecular weight, elemental and structural composition, oxidation state, volatility, aqueous solubility, and more. 4,27,59,67,68 These characteristics serve as metrics for comparing and apportioning BrC observed in real-world studies within the proposed opticallybased classification framework. For example, high molecular weight BrC compounds have been observed to be less susceptible to photodegradation than lower molecular weight compounds. 56,69 Another study discovered that photolyzed BrC species featured higher oxidation state values and lower molecular weights, demonstrating photooxidation aging mechanisms during long-range transport. 70 Recent laboratory studies have also reported changes in the composition and reactivity of BrC mixtures resulting from the evaporation of their components.<sup>71–73</sup> However, establishing a predictive understanding of BrC's molecular composition and light absorption properties is yet incomplete, necessitating additional comprehensive studies. Notably, even trace amounts of strongly absorbing chromophores can contribute significantly to the overall optical properties of bulk BrC material. 4,33,36,37,74,75 Therefore, elucidating this intricate relationship requires the application of complementary multi-modal analytical techniques that can measure both component-specific and bulk BrC properties.

A hyphenated analytical platform that combines high performance liquid chromatography (HPLC), photodiode array (PDA) detector, and high-resolution mass spectrometer (HRMS) has emerged as the preferred method for molecular-level and chromophore-specific characterization

of BrC.<sup>23,39,40,45,60–62,76–82</sup> However, this approach relies on the extraction efficiency of BrC in solvents, which is often incomplete. Moreover, even assuming complete extraction of BrC materials, the optical properties of bulk BrC do not fully replicate aerosolized BrC, as light extinction by airborne particles is influenced by the size distribution and micro-physical properties of particles.<sup>85</sup> To develop a comprehensive and atmospherically relevant understanding of BrC's optical characteristics, it is imperative to investigate aerosols generated from the same BrC source material using broadband optical measurements of size-resolved airborne particles.<sup>33,36,86–88</sup> Our new approach of modifying bulk phase BrC constituents with thermal evaporation experiments enables us to better mimic BrC chemical and optical properties in the aerosol phase and take advantage of the optical measurements and accurate molecular characterization offered by the HPLC-PDA-HRMS technique. This incorporation of HPLC-HRMS measurements is a comprehensive approach that enhances our understanding of BrC's evolution in the atmosphere.

# 2. EXPERIMENTAL

2.1. Generation of BrC tar condensates. Smoke emissions from pyrolysis of hardwood pellets (Hallingdal Trepellets, water content 7-8%, 2-3 cm length, 8 mm diameter) were flown through a 20 °C water-circulating condenser and were collected into a glass impinger. This experimental setup is described in Supplemental Note 1, Figure S1. This pyrolysis process, which occurs deep in the pores of burning plants where oxygen concentration is low and temperatures are highly elevated, was conducted using dry N<sub>2</sub> gas blown through a 1 L Pyrex round-bottom flask residing in an electric heater set to ~550 °C for the experiment. S6,89,90 Smoke fumes comprising condensable species at room temperature and water-soluble gases were captured in the impinger, resulting in the formation of a liquid condensate. However, certain gas-phase species with low water solubility might have escaped through the impinger's exhaust. The composition and optical properties of the

collected condensate resemble BrC constituents from biomass burning. <sup>36,91</sup> The collected liquid condensate was transferred to a separatory funnel, where the condensate self-separated into immiscible "aqueous" and "oily" fractions. Chemical characterization of both fractions indicated that constituents of the aqueous fraction were a subset of the more complex oily fraction. <sup>62</sup> Hence, the oily fraction of the condensate was isolated and used in this study, referenced here as a primary wood Pyrolysis Oil (PO<sub>1</sub>). Three aliquots of PO<sub>1</sub> (each of 10 mL volume) were placed in individual 20 mL amber vials (I.D.: 27.5 mm, Height: 57 mm) heated to ~350 °C with a flow of N<sub>2</sub> gas passing over the heated mixtures to facilitate evaporation of their volatile components. Each of the aliquots was heated for different periods of time. Corresponding volume reduction factors of 1.25 (75% volume remaining, 20 min heating), 2 (50% volume remaining, 40 min heating), and 3 (33% volume remaining, 80 min heating) were calculated by measuring each aliquot's decrease in height in the vials with a caliper. These reduction factors were used to index the new evaporated samples as PO<sub>1.25</sub>, PO<sub>2</sub>, and PO<sub>3</sub>. All PO<sub>x</sub> samples were kept in individual vials, sealed with parafilm, wrapped in aluminum foil, and stored in the dark at ~20 °C in a freezer until further analysis.

2.2. Measurement of bulk and aerosolized sample optical properties. Solutions of PO<sub>x</sub> samples in acetonitrile (Optima LC-MS grade, Fisher Chemical) were prepared with individual concentrations in a range of 30-60 μg/mL and their UV-Vis absorption spectra were measured using a spectrophotometer (Ocean Optics Model DH-2000). To ensure consistent comparison across PO<sub>x</sub> samples, we selected acetonitrile (polarity index of 5.8) as the extraction solvent. This selection was made based on its proven efficiency in extracting a wide range of PO components, <sup>37,40,62</sup> inertness with our analytes, <sup>92,93</sup> and its compatibility with the LC separation method used. <sup>40,62</sup> These factors collectively enhance the comparability with previously reported findings. <sup>37,40,62,94</sup> The absorption spectrum of each bulk PO<sub>x</sub> solution is reported in terms of the

wavelength-dependent mass absorption coefficient (MAC( $\lambda$ )<sub>bulk</sub>),<sup>95</sup> which is calculated from the log<sub>10</sub>-base absorbance (Abs( $\lambda$ )<sup>soln</sup>), optical path length (l=0.01 m), and concentration of organic mass (C<sub>OM</sub>(g/m<sup>3</sup>)).

$$MAC(\lambda)_{bulk}(m^2 g^{-1}) = \frac{Abs(\lambda)^{soln}(AU) \times \ln(10)}{l(m) \times C_{OM}(g m^{-3})}$$
(1)

This calculation assumes that the entire  $PO_x$  sample consists of organic mass ( $C_{OM}$ ) and the evaporation step does not generate solvent-insoluble colloids.

The PO<sub>x</sub> solutions in acetonitrile at higher concentrations of  $\sim 3$  g/L were used to aerosolize BrC particles using a constant output TSI atomizer (Model 3070). To facilitate removal of the acetonitrile solvent, the generated aerosol was directed through a quartz furnace (I.D.: 7.5 mm, Length: 20 cm, Temperature settings: 250 °C) followed by a series of charcoal denuders. The extinction of light by solvent-free BrC aerosols was measured using a custom-built broadband cavity-enhanced spectrometer (BBCES), described in detail elsewhere.<sup>36</sup> Briefly, the BrC particles were initially size-selected with an Aerodynamic Aerosol classifier (AAC) (Cambustion, UK). Subsequently, the flow of monodispersed particles was equally distributed to a condensation particle counter (CPC) (model 3775, TSI), a scanning mobility particle spectrometer (SMPS) (classifier 3080, DMA 3081, CPC 3775low, TSI), and the BBCES. The CPC quantified particle number concentration, SMPS captured mobility size distribution, and the BBCES monitored particle wavelength-resolved light extinction in a range of 315-650 nm (315-350 nm and 365-650 nm with a resolution of 0.5 nm). Aerosol samples were collected on preweighed Teflon filters (PM<sub>2.5</sub> PTFE membrane, 46.2 mm diameter, Whatman Inc.). Captured PO<sub>x</sub> aerosols were extracted from the filters using acetonitrile (at concentrations of 25-40 µg/mL) and remeasured with a UV-Vis spectrophotometer to determine MAC( $\lambda$ )<sub>aerosol</sub>. Based on the Mie theory and size-wavelengthresolved particle extinction coefficients, the intrinsic refractive index (RI=n+ik, where n represents

the real part for scattering and k denotes the imaginary part for absorption) was retrieved. The density of  $1.25 \pm 0.03$  g/mL for these aerosols was measured directly by the AAC-SMPS, assuming spherical, homogenous particles (see Figure S2 in Supplemental Note 2 for more details).

$$k(\lambda) = \frac{MAC(\lambda)_{aerosol} \times \rho_{aerosol} \times \lambda}{4\pi}$$
 (2)

The absorption Ångstrom exponent (AAE) was calculated to reflect the wavelength dependence of  $MAC(\lambda)_{bulk}$ .

$$MAC(\lambda)_{bulk} = k \times \lambda^{-AAE}$$
 (3)

The AAE values were calculated by measuring the slope of the log-log plot of MAC( $\lambda$ )<sub>bulk</sub> vs wavelength across 300-500 nm.<sup>62</sup>

2.3. HPLC-PDA-HRMS Analysis. PO<sub>1</sub>, PO<sub>1.25</sub>, PO<sub>2</sub>, and PO<sub>3</sub> samples were dissolved in acetonitrile to obtain similar 5 mL stock solutions at ~2000 μg/mL concentration. 500 μL aliquots were filtered through prewetted 0.2 μm sieve, 17 mm diameter PTFE (hydrophobic) filter syringes (ThermoFisher Scientific). Additionally, a vacuum-evaporated PO<sub>2</sub> sample was prepared by storing a PO<sub>1</sub> sample in a vacuum oven for 3 days at 25 °C under high vacuum to evaporate volatile PO constituent molecules (refer to Supplemental Note 2, Figure S3 for additional details). This experiment was conducted to validate that the optical and chemical properties of the heated samples were attributed to the removal of volatile constituents rather than chemical reactions facilitated by increased temperature. All five PO<sub>x</sub> samples (PO<sub>1</sub>, PO<sub>1.25</sub>, PO<sub>2</sub>, PO<sub>3</sub>, and vacuum-evaporated PO<sub>2</sub>) were analyzed using a Vanquish HPLC system connected to a LightPipe flow cell and high-resolution Orbitrap mass spectrometer Q Exactive HF-X (all from Thermofisher Scientific). The HPLC separation was performed using a reversed-phase Luna C18 column (Phenomenex, 00F-4252-B0) and a SecurityGuard C18 Guard Cartridge (Phenomenex, AJO-4286).<sup>62</sup> An injection volume of 5 μL was used for all ~2000 μg/mL samples, and the column was

maintained at 25 °C. We employed a previously established elution protocol using a mobile phase mixture of water with 0.1% v/v formic acid (A) and acetonitrile with 0.1% v/v formic acid (B) at a flow rate of 0.2 mL/min.<sup>62</sup> The following gradient was applied: 0-3 min at 90% of A, 3-90 min a linear gradient to 0% of A, 90-100 min maintained at 0% A, and 101-120 min held at 90% of A to re-equilibrate the column for the next analysis run.<sup>62</sup> The eluent first flowed through the PDA detector, followed by the HRMS detector. The PDA detector contained a 1.0 cm fused-silica LightPipe flow cell, a deuterium lamp light source, and recorded an absorbance between 200-680 nm at a scan rate of 20 Hz and a spectral resolution of 2 nm. Measurements using an acetonitrile blank were acquired to remove optical and chemical background interferences associated with the mobile phase itself. Electrospray (ESI) and dopant-assisted atmospheric pressure photoionization (APPI) sources in both positive and negative modes were used to detect polar and nonpolar chromophores. 40,60,62 The following ESI settings were employed: 250 °C capillary temperature, 200 °C probe temperature, 3.5 kV spray voltage, 35 units of sheath gas, 10 units of auxiliary gas, and 1 unit of sweep gas. For APPI, the ion source was equipped with a krypton lamp (Syagen Photomate), the vaporizer temperature was set at 400 °C and the spray voltage was increased up to 5.0 kV. The dopant consisted of 3-trifluoromethylanisole (TFMA; 98% purity, Alfa-Aesar) and chlorobenzene (anhydrous, 99.8% purity, Sigma-Aldrich) at a 1:99 v/v ratio and the dopant flow (0.02 mL/min) was added to the HPLC outflow upstream of the ionization zone. 96,97 Calibration of the MS detector was performed using commercial solutions (Thermo Scientific, PI-88323 and PI-88324) ionized in ESI mode in both polarities.

2.4. Calculation of MAC and AAE from PDA records.  $MAC(\lambda)$  values corresponding to the total light absorption for each of the individual  $PO_x$  samples were calculated from their corresponding HPLC-PDA measurements using the following equation.<sup>98</sup>

$$MAC(\lambda)_{\Sigma}^{PDA}(m^2 g^{-1}) = \frac{Abs(\lambda)_{\Sigma}^{PDA} \times \Delta t \times \ln(10) \times F}{b \times 10 \times m_{ini}}$$
(4)

Where: Abs $(\lambda)_{\Sigma}^{PDA}$  (µAU) represents the absorbance recorded at wavelength  $\lambda$  integrated over the entire elution time, Δt reflects the elution time range (0-100 min), F represents the LC flow rate (0.2 mL/min), b is the pathlength of the Lightpipe flow cell (1.0 cm), and mini corresponds to the injected mass (9800 ng) of the POx samples. The unit conversions from µAU to AU, cm3 to m<sup>3</sup>, cm to m, and ng to g units are accomplished by applying the coefficient 10.62,98,99 BrC chromophores were distinguished between three broad fractions based on elution time ranges, informed by the PO<sub>1</sub> molecular characterization reported in our previous study.<sup>62</sup> Fraction A (3-40 min) comprised the most polar analytes including single-ring species, like methoxyphenols and furans; Fraction B (40-65 min) included medium-polarity compounds, broadly termed as lignin decomposition products; and Fraction C (65-100 min) featured the least polar constituents, such as heteroatom-containing polycyclic aromatic hydrocarbons (PAHs) with three or more rings. 62 Supplemental Note 2, Figures S4-S5 provide detailed descriptions of absorbance contributions for these three fractions of BrC chromophores and how they contribute specifically to absorbance in the UV and visible regions. The relative contributions of  $MAC(\lambda)_i^{PDA}$  attributable to each of these three fractions were computed using equation 5.

$$MAC(\lambda)_{i}^{PDA}(m^{2} g^{-1}) = MAC(\lambda)_{\Sigma}^{PDA} \times \left[\frac{Abs(\lambda)_{i}^{PDA} \times \Delta t_{i}}{Abs(\lambda)_{\Sigma}^{PDA} \times \Delta t_{\Sigma}}\right]$$
 (5)

Here, the  $MAC(\lambda)_i^{PDA}$  represents the integrated UV-Vis absorbance of the specific fraction i and  $\Delta t_i$  is its elution time period. The wavelengths of interest ranged from 300-500 nm, which is primarily UV-A up to the visible light wavelength range. The relative contributions of unretained species, eluting over 0-3 min of the separation runs, were also quantified in a similar manner.

2.5. Chemical compositional analysis. Background-subtracted HPLC-HRMS datasets acquired for the PO<sub>x</sub> samples were evaluated using MZMine 2.53, an open source software for

LC-MS processing (<a href="https://mzmine.github.io">https://mzmine.github.io</a>). <sup>100</sup> HRMS data was acquired across a mass range of 80-1200 m/z with a mass resolution of 240,000 at 200 m/z. Supplemental Note 3 provides a detailed explanation on how extracted ion chromatograms (EICs) were generated to identify masses in the PO<sub>x</sub> samples.

Elemental formulas corresponding to the individual peaks detected in each of the PO<sub>x</sub> samples were first grouped into homologous series using custom-built macro Excel files<sup>101</sup> and then assigned using the MIDAS molecular formula calculator (v. 1.2.3; National High Magnetic Field Laboratory, USA). Formula assignments permitted unrestricted counts of C and H atoms, up to 50 O atoms, and up to 3 N atoms. The assignments were limited to single-charged ions. Initial assignments were deemed erroneous based on one or all of the following factors: a double bond equivalency (DBE) value above the 0.9×C limit, a completely aliphatic compound with a DBE value = 0, or the assigned compound lied outside the error clustering trend. For ions detected in ESI(+) mode, one Na atom was permitted for assignments of MS features detected. All other ionization modes permitted up to 1 S atom. Assignments in APPI(+) and APPI(-) modes permitted radical cations and radical anions, respectively. Once assignments are made for the ions, they are classified into five different groups: CH, CHO, CHNO, CHN, and S-containing. Figures S6-S7 in Supplemental Note 3 display the fractional mass spectra of the PO<sub>x</sub> samples and UpSet graphs summarizing the ions detected and assigned for each of the PO<sub>x</sub> samples (excluding the vacuumevaporated PO<sub>2</sub> sample) in both positive and negative ionization modes. The chemical composition of the additional PO<sub>2</sub> sample created through vacuum evaporation at room temperature was compared to the one generated via thermal evaporation. The results of this comparative chemical characterization are shown in Figure S8. Supplemental Note 4, Figures S9-S10 describe the DBE trends of assigned molecules in the PO<sub>x</sub> samples and the quantity of potential detected BrC

chromophores present in the samples. 40,102 Supplemental Note 5, Figures S11-S13 describe the abundance of oxygen-containing moieties and extent of oxidized CHO compounds through the application of maximum carbonyl ratio - van Krevelen (MCR-VK) diagrams. 103,104 In addition, Figure S14 and Table S1 describe the extent of CHO and CHNO species through the use of nominal oxidation state of carbon (NOS<sub>C</sub>) metric. 105

The estimated volatilities of the CHO and CHNO compounds according to their logarithmic values of saturation vapor pressure mass concentrations ( $\log_{10}(C_0, \mu g/m^3)$ ) are calculated with the following equation.

$$\log_{10}(C_0) = (n_C^0 - n_C)b_C - n_O b_O - 2\frac{n_C n_O}{n_C + n_O}b_{CO} - n_N b_N$$
(6)

The reference carbon numbers  $(n_C^0)$  and b coefficients for CHO and CHNO species are reported in Table 1 in Li et al. 2016. <sup>106</sup>

The viscosities of the CHO and CH species ( $log_{10}(\eta, Pa \cdot s)$ ) are estimated using the Vogel-Tammann-Fulcher equation.<sup>107</sup>

$$\eta = \eta_{\infty} e^{\frac{T_0 D}{T - T_0}} \tag{7}$$

Where:  $\eta_{\infty}$  (Pa·s) represents the low limit viscosity value (10<sup>-5</sup> Pa·s) at very high temperatures; T is the ambient temperature (298 K); T<sub>0</sub> is the Vogel temperature calculated as T<sub>0</sub> =  $39.17 \times T_g/(D+39.17)$ . Here, D is the fragility parameter, which describes the rate at which the dynamics of the compound slows down as T approaches the material's glass transition  $T_g$  temperature. The T<sub>g</sub> values of individual species are estimated from their elemental formulas using the parameterization approach summarized in Supplemental Note 7. Equations 6 and 7 are used together to identify volatility and viscosity trends in detected compounds as the PO<sub>1</sub> sample progressively evaporates into PO<sub>3</sub>.

# 3. RESULTS AND DISCUSSION

Figure 1 illustrates HPLC-PDA heatmaps chromatograms for each of the PO<sub>x</sub> samples shown in the left-hand side panels, while the right-hand panels illustrate how MAC( $\lambda$ )<sub>1</sub>PDA of each fraction contribute to the total MAC( $\lambda$ )<sub>2</sub>PDA values. BrC chromophores identified in our previous work are highlighted, with plausible structures provided by cross-referencing molecular formulas with their corresponding UV-Vis spectra and relevant literature (for the component-specific references see *Hettiyadura et al.* 2021 and references therein).<sup>62</sup> As more volatile constituents evaporate from PO<sub>1</sub> upon its conversion to PO<sub>3</sub>, the total MAC( $\lambda$ )<sub>2</sub>PDA values shift towards a stronger light-absorbing carbon sample. This shift is explained by an accumulation of MAC( $\lambda$ )<sub>1</sub>PDA in Fractions B and C, coupled with a reduction of MAC( $\lambda$ )<sub>1</sub>PDA in Fraction A.

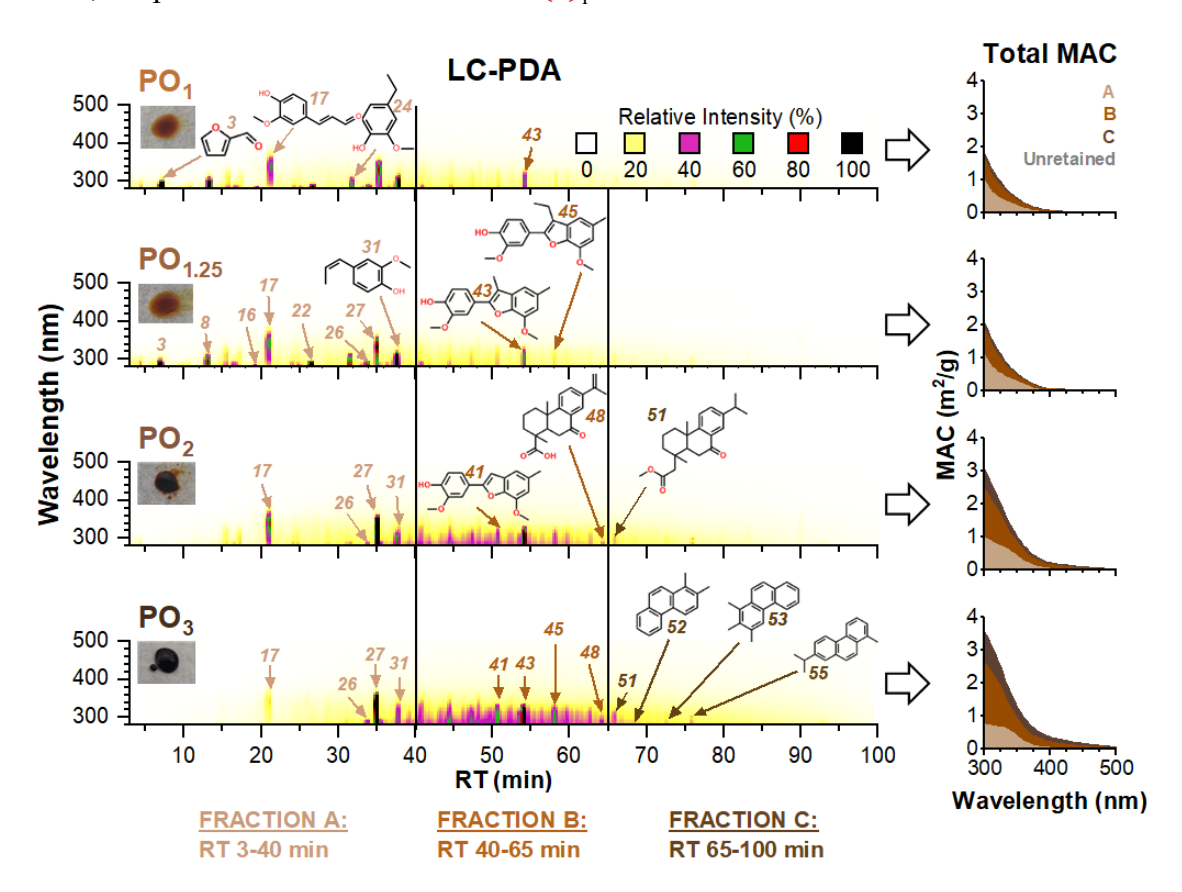


Figure 1. HPLC-PDA chromatograms of  $PO_x$  samples (left panels) and their corresponding integrated total  $MAC(\lambda)_{\Sigma}^{PDA}$  spectra (right panels) showing relative contributions of A, B, and C

fractions of BrC chromophores. Fraction A describes very polar monoaromatic chromophores, Fraction B contains semi-polar 2-3 ring fragments of lignin decomposition, and Fraction C exhibits low-polarity, multi-ring polyaromatic species. The unretained species contribute negligibly to the total  $MAC(\lambda)_{\Sigma}^{PDA}$  spectra. Structures and numeric IDs are reproduced from Hettiyadura et al. 2021.62

Figure 2 exhibits the total MAC plots of the  $PO_x$  samples as measured by the UV-Vis spectrophotometer (solution phase), PDA detector (solution phase), and the BBCES instrument (aerosol phase). As volatile constituents degas from  $PO_1$  and the bulk material transitions to  $PO_3$ , the mixture's  $MAC(\lambda)_{bulk}$  and  $MAC(\lambda)_{\Sigma}^{PDA}$  values are enhanced in the solution phase. Conversely, all aerosolized  $PO_x$  samples exhibit very similar  $MAC(\lambda)$  values according to the BBCES instrument, indicating that aerosolization led to the evaporation of volatile constituents, enhancing the absorbance of the particle-phase BrC materials. Notably, the evaporation process was further augmented by conditioning the  $PO_x$  aerosol flow through a heated inlet connected to a charcoal denuder positioned before the BBCES. This setup effectively removed additional organic compounds that might have otherwise remained in the aerosol phase under ambient conditions. Additionally, the filtration of insoluble BrC components by the LC guard cartridge may alter the differences between PDA and BBCES records.

Bulk PO<sub>1</sub> and PO<sub>1.25</sub> samples, which experienced only a marginal loss of volatile compounds, display solution-phase MAC( $\lambda$ ) values that are significantly lower than the aerosolized MAC( $\lambda$ ) values measured by the BBCES instrument. Conversely, the bulk PO<sub>2</sub> and PO<sub>3</sub> samples, which experienced significant evaporation of more volatile species, exhibit solution-phase MAC( $\lambda$ ) values that approach their corresponding aerosolized MAC( $\lambda$ ) values. These findings agree with our previous report, indicating that aerosolized BrC materials pose higher MAC( $\lambda$ ) values than their solution-phase counterparts.<sup>62</sup> These findings agree with other studies that have also reported that lab-generated BrC constituents undergo darkening and a decrease in single-scattering albedo

upon aerosolization. $^{66,110}$  This convergence of the MAC( $\lambda$ ) values measured for aerosolized PO samples and their corresponding heated bulk samples underscores that darkening of BrC aerosols through volatilization can be achieved by heating the oily phase of the BrC condensate before conducting optical measurements. $^{62}$  Preparing and measuring the oily phase fraction of BrC condensate in this manner may facilitate more accurate measurements of BrC aerosol optical properties, informing atmospheric models.

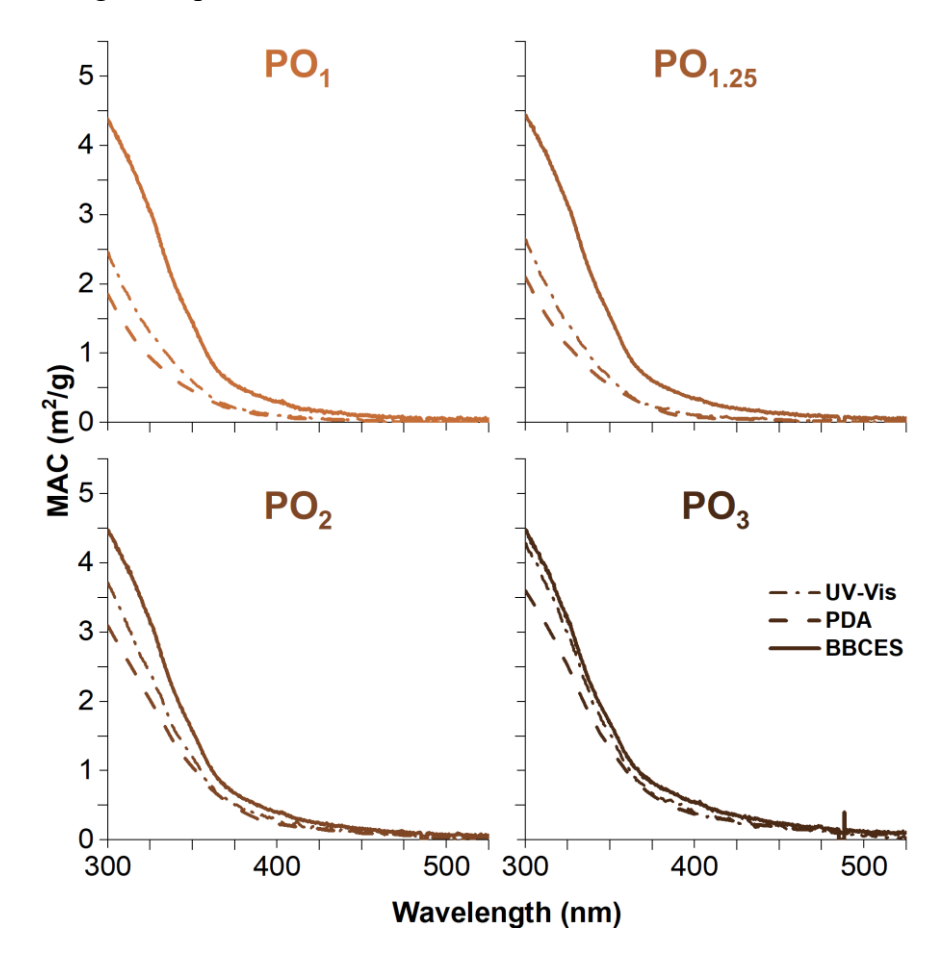


**Figure 2.** Comparison of MAC( $\lambda$ ) values between solution-phase and aerosol-phase PO<sub>x</sub> samples. PO<sub>1</sub> and PO<sub>1.25</sub> samples exhibit a significant disparity in MAC( $\lambda$ ) values between aerosol and bulk solution. PO<sub>2</sub> and PO<sub>3</sub> demonstrate closely matched MAC( $\lambda$ ) values in both phases, indicating that the optical properties of the oily phase fraction of BrC condensate can emulate those of BrC aerosol through the "darkening-by-volatilization" process. <sup>62</sup>

To visualize the BrC transformations in these samples, the optical properties of the PO<sub>x</sub> samples were evaluated using the AAE versus log<sub>10</sub>(MAC<sub>405 nm</sub>) optical classification framework,<sup>59</sup> shown in Figure 3, where AAE values were obtained from the slopes of the ln(MAC) vs ln(λ) plots across the 300-500 nm wavelength range. This figure effectively illustrates the shift towards stronger absorbing BrC materials from PO<sub>1</sub> to PO<sub>3</sub>. As our measurements transition from solution-phase PO<sub>1</sub> to aerosol-phase PO<sub>3</sub>, AAE and log<sub>10</sub>(MAC<sub>405 nm</sub>) values shift from approximately 11 to 7 and from -1 to 0.3, respectively. Figure 3 indicates that AAE and MAC<sub>405 nm</sub> values of the evaporated PO<sub>x</sub> samples exhibit transformation of their BrC classification from the VW-BrC to a stronger absorbing W-BrC optical bin, demonstrating the "darkening-by-volatilization" process. The evaporation of small constituent molecules corresponds to an enrichment of strongly absorbing BrC materials in the PO<sub>3</sub> sample. This darkening phenomenon has been reported in other literature as well.<sup>60,61,111</sup>

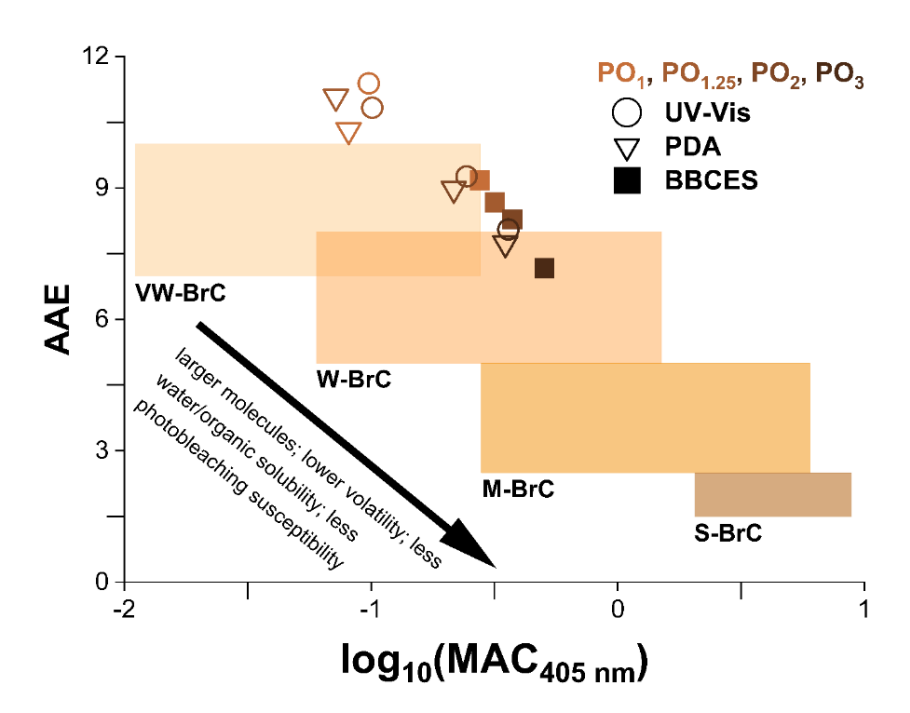


**Figure 3.** Classification of  $PO_x$  samples according to the optical framework of Saleh 2020.<sup>59</sup> The  $PO_1$  sample is allocated to the VW-BrC optical bin, considering its MAC<sub>405 nm</sub> values, while those values of the  $PO_3$  sample are shifted into the W-BrC optical bin.

We conducted estimates of individual volatility and viscosity values for assigned compounds, summarized for each of the A, B, and C fractions in the PO<sub>x</sub> samples, and correlated them with the corresponding fractional MAC( $\lambda$ ) plots, as shown in Figure 4. Volatilities (expressed as saturation vapor pressures at room temperature,  $C_0$ , in units of  $\mu g/m^3$ ) were estimated using molecular corridor calculations for all individual CHO and CHNO species detected in the PO<sub>x</sub> samples. 106 The extended plots summarizing these calculated component-specific records are included in Supplemental Note 6, Figures S15-S16 and Tables S2-S3. Results of these calculations were used to categorize organic compounds into five common volatility bins based on their  $log_{10}(C_0)$  values: volatile organic compounds (VOC,  $log_{10}(C_0) > 6.48$ ), intermediate volatility organic compounds (IVOC,  $6.48 > \log_{10}(C_0) > 2.48$ ), semi volatile organic compounds (SVOC,  $2.48 > \log_{10}(C_0) > -$ 0.52), low-volatility organic compounds (LVOC,  $-0.52 > \log_{10}(C_0) > -3.52$ ), and extremely lowvolatility organic compounds (ELVOC,  $-3.52 > \log_{10}(C_0)$ ). The volatility distributions and their mean values shown in Figure 4b demonstrate systematic changes across the PO<sub>x</sub> samples, indicating a shift from the mostly IVOC compounds in PO1 to the much less volatile SVOC and even LVOC species in PO<sub>3</sub>, aligning with the removal of small volatile constituents in the PO<sub>1</sub> sample. Accumulation of low volatility species in the progression of PO<sub>1</sub> to PO<sub>3</sub> samples aligns with the enhanced absorbance of these samples, as evidenced from Figure 4a, supporting the darkening through volatilization mechanism suggested in our previous study<sup>62</sup> and corroborated by field observations. 112-116

The glass transition temperatures of individual species were calculated and used to estimate the viscosity ranges of the PO<sub>x</sub> samples. Viscosity is an important physicochemical property of aerosols, which affects rates of heterogeneous chemistry, uptake of gas-phase species, and photodegradation. <sup>117–122</sup> Details of these calculations <sup>108,109</sup> and the extended plots summarizing the

component-specific viscosity values are included in Supplemental Note 7, Figure S17 and Table S4. Based on these calculations, BrC constituents were categorized as solid (>10<sup>12</sup> Pa·s), semi-solid (10<sup>12</sup>-10<sup>2</sup> Pa·s), or liquid (<10<sup>2</sup> Pa·s). The most viscous components are the lignin fragments (Fraction B), as evidenced by their mean values and distributions displayed in Figure 4c. The smaller, least viscous constituents of Fraction A evaporate from the PO<sub>1</sub> sample causing progressively higher viscosities estimated for the PO<sub>1.25</sub>, PO<sub>2</sub>, and PO<sub>3</sub> samples. Notably, the more viscous constituents of Fraction B collectively contribute to stronger light absorption, as measured by the PDA detector (Figure 1). The widths of the boxes in the volatility (Figure 4b) and viscosity (Figure 4c) plots are scaled based on the intensity of species detected in the corresponding fractions (A, B, and C), illustrating that volatile, liquid-like constituents of Fraction A evaporate from the PO<sub>1</sub> sample, while less volatile, semi-solid-like components of Fraction B and C accumulate in the PO<sub>1.25</sub>, PO<sub>2</sub>, and PO<sub>3</sub> samples.

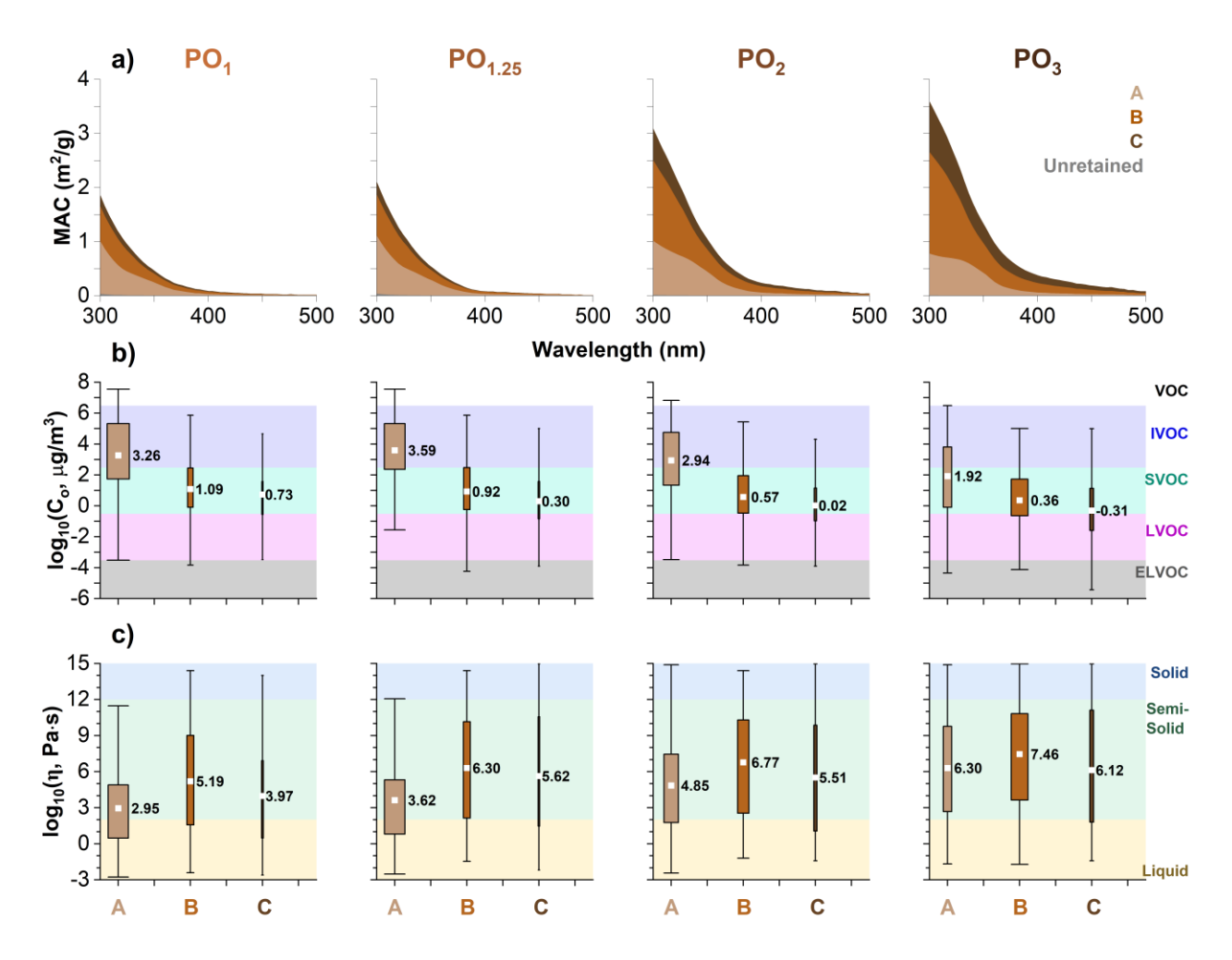


**Figure 4.** Panel a: Fractional MAC( $\lambda$ ) plots for PO<sub>x</sub> samples. Panel b: Saturation vapor pressure box-and-whisker plots featuring whiskers with lengths equal to 1.5 × interquartile range. Volatility plots represent all CHO and CHNO compounds detected by the HRMS. Panel c: Viscosity box-and-whisker plots featuring whisker lengths equal to 1.5 × interquartile range, mean values are shown, and outliers are not displayed. Viscosity distributions exhibit CHO and CH species. In panels b and c, box widths are scaled based on the intensity-weighted ratios of compounds detected in each fraction (A, B, and C). As the absorbance increases across the progression of PO<sub>1</sub> to PO<sub>3</sub> samples, the volatility box-and-whisker distributions shift from IVOC/SVOC bins towards lower volatility SVOC/LVOC categories. Simultaneously, the viscosity distributions shift from the liquid/semi-solid range towards the semi-solid viscosity range. The box widths of Fraction A species shrink (they become less abundant) while the box widths of Fractions B and C species increase (they become more abundant species).

#### ATMOSPHERIC IMPLICATIONS

One of the primary findings of this study is that subjecting the PO<sub>x</sub> material to evaporation increased the light absorption properties of the remaining condensed-phase fractions progressively

becoming similar to their aerosolized counterparts. This observation underlines the significance of the gas-particle partitioning dynamics in accurately characterizing the optical properties of BrC aerosols. Furthermore, the high surface-to-volume ratio and small sizes of atmospheric accumulation mode particles suggest that evaporation of IVOC components can occur very rapidly. For instance, the equilibrium e-folding times of 200 nm particles, assuming a range of  $\sim 10^3$  Pa·s to  $\sim 10^6$  Pa·s viscosities reported here (Figure 4c), are on the time scale of seconds and minutes, respectively. 124 Therefore, for these particles, gas-particle partitioning is not limited by slow diffusion even in the viscous (~10<sup>2</sup> Pa·s) particles. It follows that darkening of BrC aerosol by evaporation takes place at a timescale shorter than the aerosol lifetime and its atmospheric multiphase reaction chemistry. Various field studies report that viscous and highly absorbing tar ball particles are commonly found in BB smoke plumes after prolonged atmospheric aging. 112-116 Our findings suggest that future observations of tar balls and their buildup in BB smoke plumes need to consider the combined effects of evaporation and reaction chemistry. In this context, it is important to note that the very high absorption coefficients reported for tar balls and other refractory particles, based on electron energy-loss spectra acquired under high vacuum conditions in electron microscopy studies, 41,66,116,125,126 are likely considerable overestimates with limited relevance to particles in real atmospheric conditions.

Optical measurements and chemical characterization results presented in this study reveal that the loss of small monoaromatic compounds leads to the accumulation of larger lignin decomposition fragments and substituted PAHs, enhancing the overall absorbance of BrC mixtures. At the same time, volatility and viscosity of these mixtures also evolve, preserving less volatile and more viscous constituents, consequently augmenting overall absorbance of the BrC mixtures. It is important to note that the curved surfaces of aerosol particles and possible phase

separations within individual particles could influence the evaporation dynamics of different BrC components. This may potentially enhance the actual MAC(λ) values of aged aerosols, which may not have been fully captured in our evaporation experiments conducted on isolated oily flat surfaces. Regardless, the darkening trend observed in our experiments, is in alignment with the phenomenon of darkening through volatilization observed in both laboratory experiments<sup>62</sup> and field studies, <sup>112–116</sup> consolidating the validity of our results. Furthermore, aged BrC aerosols characterized by accumulated viscous, stronger absorbing less polar components, <sup>83,84</sup> present a challenge for chemical analysis using dissolution in common organic solvents. An advanced chemical analysis of these mixtures will necessitate systematic sequential dissolution experiments, <sup>127</sup> using a variety of solvents with different polarities and their combinations. Such an approach would enable a more comprehensive and detailed understanding of these compounds.

The implications of our study extend to various atmospheric processes. BrC aerosols that undergo darkening and become more viscous play a significant role in atmospheric processes including radiative forcing, hygroscopicity, and heterogeneous chemistry. For instance, viscous, solid-like particles have been observed to be effective carriers of absorbed harmful compounds and shielding them from oxidants and degradation processes. Additionally, solid particles can influence nucleation mechanisms in processes of mixed-phase cloud formation, favoring heterogeneous ice nucleation over homogeneous ice nucleation, which has implications for cloud formation and precipitation. Moreover, the expected increase in mixing timescales of organic compounds in solid-like particles due to hindered bulk diffusion coefficients affect atmospheric multi-phase reaction chemistry. More rigid, viscous aerosols undergo slower photochemical transformations and ozonolysis, 26,73 contributing to their chemical inertness as they disperse away from the emission source. This inertness can further amplify their absorbance

contribution in radiative forcing processes, making them a crucial factor in understanding and modelling Earth's climate system.

#### ASSOCIATED CONTENT

Supplemental Note 1 and Figure S1 describe the wood pyrolysis experiment and preparation of PO<sub>x</sub> samples. Supplemental Note 2 and Figures S2-S5 describe the optical measurements of the aerosolized PO<sub>x</sub> samples in the BBCES instrument, the HPLC-PDA separation and fractional MAC(λ) plots of the vacuum-evaporated PO<sub>2</sub> sample, the HPLC-PDA chromatograms visualizing the presence of strong and weak absorbers in each of the PO<sub>x</sub> samples, and the absorbance contributions of each BrC fraction in the UV and visible region for all PO<sub>x</sub> samples. Supplemental Note 3 describes the employed methodology to analyze HPLC-HRMS datasets using EICs. The obtained fractional mass spectra of the PO<sub>x</sub> samples are summarized in Figure S6. The UpSet graphs that illustrate the abundance of compounds detected in singular ionization modes and those detected across multiple ionization modes are presented in Figure S7. The high-resolution mass spectra comparing composition of two PO<sub>2</sub> samples obtained in thermal and vacuum evaporation experiments are displayed in Figure S8. Supplemental Note 4 and Figures S9-S10 provide information on the fractional DBE plots developed for the PO<sub>x</sub> samples and the abundance of potential BrC chromophores and aliphatic species present in Fractions A, B, and C for all PO<sub>x</sub> samples. Supplemental Note 5 and Figures S11-S13 display the MCR-VK plots for the PO<sub>x</sub> samples and the abundances of CHO compounds that belong to each of the five degree of oxidation bins and the four MCR bins for all samples. In addition, Figure S14 displays the NOSc calculated metrics and distribution of these values, while Table S1 reports the intensity-weighted averages of C number and NOSc for Fractions A, B, and C for all four PO<sub>x</sub> samples. Supplemental Note 6,

Figures S15-S16, and Tables S2-S3 display the molecular corridor diagrams developed for all PO<sub>x</sub> samples; intensity-weighted averages of volatility and molar mass of compounds in Fractions A, B, and C; abundances of compounds belonging to each of the five volatility bins; and important metrics regarding the volatility distributions. Supplemental Note 7, Figure S17, and Table S4 provide detailed information on the viscosity calculations and the distribution of viscosities in A, B, and C fractions for all four PO<sub>x</sub> samples.

#### **Author Contributions**

D.C.-A., C.L., Y.R., and A.L. designed the study. C.L. executed sample generation and sample collection tasks of the study. D.C.-A., A. M., A.P.S.H, and T.M.E. performed the molecular characterization experiments. D.C.-A. performed subsequent data analysis. C.L. performed optical measurements in experiments with aerosolized samples and analyzed corresponding data. D.C.-A. and A.L. wrote the manuscript with contributions from all co-authors A.L. and Y.R. secured grant support for this study and managed the project.

# **Notes**

There are no conflicts to declare.

# **ACKNOWLEDGMENT**

This research was supported by the international collaboration grant from US National Science Foundation (NSF Grant no. AGS-2039985) US-Israel Binational Science Foundation (BSF Grant no. 2020656), and the Israel Science Foundation (Grant #928/21).

#### REFERENCES

- (1) Washenfelder, R. A.; Attwood, A. R.; Brock, C. A.; Guo, H.; Xu, L.; Weber, R. J.; Ng, N. L.; Allen, H. M.; Ayres, B. R.; Baumann, K.; Cohen, R. C.; Draper, D. C.; Duffey, K. C.; Edgerton, E.; Fry, J. L.; Hu, W. W.; Jimenez, J. L.; Palm, B. B.; Romer, P.; Stone, E. A.; Wooldridge, P. J.; Brown, S. S. Biomass Burning Dominates Brown Carbon Absorption in the Rural Southeastern United States. *Geophys. Res. Lett.* **2015**, *42* (2), 653–664. https://doi.org/10.1002/2014GL062444.
- (2) Tian, J.; Wang, Q.; Ni, H.; Wang, M.; Zhou, Y.; Han, Y.; Shen, Z.; Pongpiachan, S.; Zhang, N.; Zhao, Z.; Zhang, Q.; Zhang, Y.; Long, X.; Cao, J. Emission Characteristics of Primary Brown Carbon Absorption From Biomass and Coal Burning: Development of an Optical Emission Inventory for China. *J. Geophys. Res. Atmos.* **2019**, 2018JD029352. https://doi.org/10.1029/2018JD029352.
- (3) Andreae, M. O.; Gelencsér, A. Black Carbon or Brown Carbon? The Nature of Light-Absorbing Carbonaceous Aerosols. *Atmos. Chem. Phys.* **2006**, *6* (10), 3131–3148. https://doi.org/10.5194/acp-6-3131-2006.
- (4) Laskin, A.; Laskin, J.; Nizkorodov, S. A. Chemistry of Atmospheric Brown Carbon. *Chem. Rev.* **2015**, *115* (10), 4335–4382. https://doi.org/10.1021/cr5006167.
- (5) Flannigan, M. D.; Krawchuk, M. A.; De Groot, W. J.; Wotton, B. M.; Gowman, L. M. Implications of Changing Climate for Global Wildland Fire. *Int. J. Wildland Fire* **2009**, *18* (5), 483. https://doi.org/10.1071/WF08187.
- (6) Parisien, M.-A.; Barber, Q. E.; Bourbonnais, M. L.; Daniels, L. D.; Flannigan, M. D.; Gray, R. W.; Hoffman, K. M.; Jain, P.; Stephens, S. L.; Taylor, S. W.; Whitman, E. Abrupt, Climate-Induced Increase in Wildfires in British Columbia since the Mid-2000s. *Commun Earth Environ* **2023**, *4* (1), 309. https://doi.org/10.1038/s43247-023-00977-1.
- (7) Peng, X.; Yu, M.; Chen, H.; Zhou, B.; Shi, Y.; Yu, L. Projections of Wildfire Risk and Activities under 1.5 °C and 2.0 °C Global Warming Scenarios. *Environ. Res. Commun.* **2023**, 5 (3), 031002. https://doi.org/10.1088/2515-7620/acbf13.
- (8) Zhang, Y.; Forrister, H.; Liu, J.; Dibb, J.; Anderson, B.; Schwarz, J. P.; Perring, A. E.; Jimenez, J. L.; Campuzano-Jost, P.; Wang, Y.; Nenes, A.; Weber, R. J. Top-of-Atmosphere Radiative Forcing Affected by Brown Carbon in the Upper Troposphere. *Nature Geosci* **2017**, *10* (7), 486–489. https://doi.org/10.1038/ngeo2960.
- (9) Calvin, K.; Dasgupta, D.; Krinner, G.; Mukherji, A.; Thorne, P. W.; Trisos, C.; Romero, J.; Aldunce, P.; Barrett, K.; Blanco, G.; Cheung, W. W. L.; Connors, S.; Denton, F.; Diongue-Niang, A.; Dodman, D.; Garschagen, M.; Geden, O.; Hayward, B.; Jones, C.; Jotzo, F.; Krug, T.; Lasco, R.; Lee, Y.-Y.; Masson-Delmotte, V.; Meinshausen, M.; Mintenbeck, K.; Mokssit, A.; Otto, F. E. L.; Pathak, M.; Pirani, A.; Poloczanska, E.; Pörtner, H.-O.; Revi, A.; Roberts, D. C.; Roy, J.; Ruane, A. C.; Skea, J.; Shukla, P. R.; Slade, R.; Slangen, A.; Sokona, Y.; Sörensson, A. A.; Tignor, M.; Van Vuuren, D.; Wei, Y.-M.; Winkler, H.; Zhai, P.; Zommers, Z.; Hourcade, J.-C.; Johnson, F. X.; Pachauri, S.; Simpson, N. P.; Singh, C.; Thomas, A.; Totin, E.; Arias, P.; Bustamante, M.; Elgizouli, I.; Flato, G.; Howden, M.; Méndez-Vallejo, C.; Pereira, J. J.; Pichs-Madruga, R.; Rose, S. K.; Saheb, Y.; Sánchez Rodríguez, R.; Ürge-Vorsatz, D.; Xiao, C.; Yassaa, N.; Alegría, A.; Armour, K.; Bednar-Friedl, B.; Blok, K.; Cissé, G.; Dentener, F.; Eriksen, S.; Fischer, E.; Garner, G.; Guivarch, C.; Haasnoot, M.; Hansen, G.; Hauser, M.; Hawkins, E.; Hermans, T.; Kopp, R.; Leprince-Ringuet, N.; Lewis, J.; Ley, D.; Ludden, C.; Niamir, L.; Nicholls, Z.; Some, S.; Szopa, S.; Trewin, B.; Van Der Wijst, K.-I.;

- Winter, G.; Witting, M.; Birt, A.; Ha, M.; Romero, J.; Kim, J.; Haites, E. F.; Jung, Y.; Stavins, R.; Birt, A.; Ha, M.; Orendain, D. J. A.; Ignon, L.; Park, S.; Park, Y.; Reisinger, A.; Cammaramo, D.; Fischlin, A.; Fuglestvedt, J. S.; Hansen, G.; Ludden, C.; Masson-Delmotte, V.; Matthews, J. B. R.; Mintenbeck, K.; Pirani, A.; Poloczanska, E.; Leprince-Ringuet, N.; Péan, C. *IPCC*, 2023: Climate Change 2023: Synthesis Report. Contribution of Working Groups I, II and III to the Sixth Assessment Report of the Intergovernmental Panel on Climate Change [Core Writing Team, H. Lee and J. Romero (Eds.)]. IPCC, Geneva, Switzerland., First.; Intergovernmental Panel on Climate Change (IPCC), 2023. https://doi.org/10.59327/IPCC/AR6-9789291691647.
- (10) Xu, L.; Peng, Y.; Ram, K.; Zhang, Y.; Bao, M.; Wei, J. Investigation of the Uncertainties of Simulated Optical Properties of Brown Carbon at Two Asian Sites Using a Modified Bulk Aerosol Optical Scheme of the Community Atmospheric Model Version 5.3. *JGR Atmospheres* **2021**, *126* (15), e2020JD033942. https://doi.org/10.1029/2020JD033942.
- (11) Jo, D. S.; Park, R. J.; Lee, S.; Kim, S.-W.; Zhang, X. A Global Simulation of Brown Carbon: Implications for Photochemistry and Direct Radiative Effect. *Atmos. Chem. Phys.* **2016**, *16* (5), 3413–3432. https://doi.org/10.5194/acp-16-3413-2016.
- (12) Saleh, R.; Marks, M.; Heo, J.; Adams, P. J.; Donahue, N. M.; Robinson, A. L. Contribution of Brown Carbon and Lensing to the Direct Radiative Effect of Carbonaceous Aerosols from Biomass and Biofuel Burning Emissions. *JGR Atmospheres* **2015**, *120* (19). https://doi.org/10.1002/2015JD023697.
- (13) Zhang, A.; Wang, Y.; Zhang, Y.; Weber, R. J.; Song, Y.; Ke, Z.; Zou, Y. Modeling the Global Radiative Effect of Brown Carbon: A Potentially Larger Heating Source in the Tropical Free Troposphere than Black Carbon. *Atmos. Chem. Phys.* **2020**, *20* (4), 1901–1920. https://doi.org/10.5194/acp-20-1901-2020.
- (14) Brown, H.; Liu, X.; Feng, Y.; Jiang, Y.; Wu, M.; Lu, Z.; Wu, C.; Murphy, S.; Pokhrel, R. Radiative Effect and Climate Impacts of Brown Carbon with the Community Atmosphere Model (CAM5). *Atmos. Chem. Phys.* **2018**, *18* (24), 17745–17768. https://doi.org/10.5194/acp-18-17745-2018.
- (15) Zeng, L.; Zhang, A.; Wang, Y.; Wagner, N. L.; Katich, J. M.; Schwarz, J. P.; Schill, G. P.; Brock, C.; Froyd, K. D.; Murphy, D. M.; Williamson, C. J.; Kupc, A.; Scheuer, E.; Dibb, J.; Weber, R. J. Global Measurements of Brown Carbon and Estimated Direct Radiative Effects. *Geophysical Research Letters* **2020**, *47* (13), e2020GL088747. https://doi.org/10.1029/2020GL088747.
- (16) Park, D.; Barabad, M. L.; Lee, G.; Kwon, S.-B.; Cho, Y.; Lee, D.; Cho, K.; Lee, K. Emission Characteristics of Particulate Matter and Volatile Organic Compounds in Cow Dung Combustion. *Environ. Sci. Technol.* **2013**, *47* (22), 12952–12957. https://doi.org/10.1021/es402822e.
- (17) World Health Organization. *The World Health Report 2002: Reducing Risks, Promoting Healthy Life*; World Health Organization, 2002.
- (18) Loebel Roson, M.; Duruisseau-Kuntz, R.; Wang, M.; Klimchuk, K.; Abel, R. J.; Harynuk, J. J.; Zhao, R. Chemical Characterization of Emissions Arising from Solid Fuel Combustion—Contrasting Wood and Cow Dung Burning. *ACS Earth Space Chem.* **2021**, *5* (10), 2925–2937. https://doi.org/10.1021/acsearthspacechem.1c00268.
- (19) Cheng, Y.; Cao, X.; Liu, J.; Yu, Q.; Zhang, Q.; He, K. Agricultural Fire Impacts on Brown Carbon during Different Seasons in Northeast China. *Science of The Total Environment* **2023**, *891*, 164390. https://doi.org/10.1016/j.scitotenv.2023.164390.

- (20) Zelenyuk, A.; Imre, D.; Beránek, J.; Abramson, E.; Wilson, J.; Shrivastava, M. Synergy between Secondary Organic Aerosols and Long-Range Transport of Polycyclic Aromatic Hydrocarbons. *Environ. Sci. Technol.* **2012**, *46* (22), 12459–12466. https://doi.org/10.1021/es302743z.
- (21) Murray, B. J.; Wilson, T. W.; Dobbie, S.; Cui, Z.; Al-Jumur, S. M. R. K.; Möhler, O.; Schnaiter, M.; Wagner, R.; Benz, S.; Niemand, M.; Saathoff, H.; Ebert, V.; Wagner, S.; Kärcher, B. Heterogeneous Nucleation of Ice Particles on Glassy Aerosols under Cirrus Conditions. *Nature Geosci* **2010**, *3* (4), 233–237. https://doi.org/10.1038/ngeo817.
- (22) Wang, B.; Lambe, A. T.; Massoli, P.; Onasch, T. B.; Davidovits, P.; Worsnop, D. R.; Knopf, D. A. The Deposition Ice Nucleation and Immersion Freezing Potential of Amorphous Secondary Organic Aerosol: Pathways for Ice and Mixed-Phase Cloud Formation. *J. Geophys. Res.* **2012**, *117* (D16), D16209. https://doi.org/10.1029/2012JD018063.
- (23) Zhou, Y.; West, C. P.; Hettiyadura, A. P. S.; Pu, W.; Shi, T.; Niu, X.; Wen, H.; Cui, J.; Wang, X.; Laskin, A. Molecular Characterization of Water-Soluble Brown Carbon Chromophores in Snowpack from Northern Xinjiang, China. *Environ. Sci. Technol.* 2022, 56 (7), 4173–4186. https://doi.org/10.1021/acs.est.1c07972.
- (24) Shrivastava, M.; Lou, S.; Zelenyuk, A.; Easter, R. C.; Corley, R. A.; Thrall, B. D.; Rasch, P. J.; Fast, J. D.; Massey Simonich, S. L.; Shen, H.; Tao, S. Global Long-Range Transport and Lung Cancer Risk from Polycyclic Aromatic Hydrocarbons Shielded by Coatings of Organic Aerosol. *Proc. Natl. Acad. Sci. U.S.A.* 2017, 114 (6), 1246–1251. https://doi.org/10.1073/pnas.1618475114.
- (25) Zhou, S.; Shiraiwa, M.; McWhinney, R. D.; Pöschl, U.; Abbatt, J. P. D. Kinetic Limitations in Gas-Particle Reactions Arising from Slow Diffusion in Secondary Organic Aerosol. *Faraday Discuss.* **2013**, *165*, 391–406. https://doi.org/10.1039/C3FD00030C.
- (26) Schnitzler, E. G.; Gerrebos, N. G. A.; Carter, T. S.; Huang, Y.; Heald, C. L.; Bertram, A. K.; Abbatt, J. P. D. Rate of Atmospheric Brown Carbon Whitening Governed by Environmental Conditions. *Proc. Natl. Acad. Sci. U.S.A.* **2022**, *119* (38), e2205610119. https://doi.org/10.1073/pnas.2205610119.
- (27) Moise, T.; Flores, J. M.; Rudich, Y. Optical Properties of Secondary Organic Aerosols and Their Changes by Chemical Processes. *Chem. Rev.* **2015**, *115* (10), 4400–4439. https://doi.org/10.1021/cr5005259.
- (28) Hems, R. F.; Schnitzler, E. G.; Liu-Kang, C.; Cappa, C. D.; Abbatt, J. P. D. Aging of Atmospheric Brown Carbon Aerosol. *ACS Earth Space Chem.* **2021**, *5* (4), 722–748. https://doi.org/10.1021/acsearthspacechem.0c00346.
- (29) Zhang, L.; Segal-Rozenhaimer, M.; Che, H.; Dang, C.; Sedlacek Iii, A. J.; Lewis, E. R.; Dobracki, A.; Wong, J. P. S.; Formenti, P.; Howell, S. G.; Nenes, A. Light Absorption by Brown Carbon over the South-East Atlantic Ocean. *Atmos. Chem. Phys.* **2022**, *22* (14), 9199–9213. https://doi.org/10.5194/acp-22-9199-2022.
- (30) Zeng, L.; Dibb, J.; Scheuer, E.; Katich, J. M.; Schwarz, J. P.; Bourgeois, I.; Peischl, J.; Ryerson, T.; Warneke, C.; Perring, A. E.; Diskin, G. S.; DiGangi, J. P.; Nowak, J. B.; Moore, R. H.; Wiggins, E. B.; Pagonis, D.; Guo, H.; Campuzano-Jost, P.; Jimenez, J. L.; Xu, L.; Weber, R. J. Characteristics and Evolution of Brown Carbon in Western United States Wildfires. *Atmos. Chem. Phys.* 2022, 22 (12), 8009–8036. https://doi.org/10.5194/acp-22-8009-2022.
- (31) Ponczek, M.; Franco, M. A.; Carbone, S.; Rizzo, L. V.; Monteiro Dos Santos, D.; Morais, F. G.; Duarte, A.; Barbosa, H. M. J.; Artaxo, P. Linking the Chemical Composition and Optical

- Properties of Biomass Burning Aerosols in Amazonia. *Environ. Sci.: Atmos.* **2022**, *2* (2), 252–269. https://doi.org/10.1039/D1EA00055A.
- (32) Hodshire, A. L.; Akherati, A.; Alvarado, M. J.; Brown-Steiner, B.; Jathar, S. H.; Jimenez, J. L.; Kreidenweis, S. M.; Lonsdale, C. R.; Onasch, T. B.; Ortega, A. M.; Pierce, J. R. Aging Effects on Biomass Burning Aerosol Mass and Composition: A Critical Review of Field and Laboratory Studies. *Environ. Sci. Technol.* **2019**, *53* (17), 10007–10022. https://doi.org/10.1021/acs.est.9b02588.
- (33) Bluvshtein, N.; Lin, P.; Flores, J. M.; Segev, L.; Mazar, Y.; Tas, E.; Snider, G.; Weagle, C.; Brown, S. S.; Laskin, A.; Rudich, Y. Broadband Optical Properties of Biomass-burning Aerosol and Identification of Brown Carbon Chromophores. *J. Geophys. Res. Atmos.* **2017**, 122 (10), 5441–5456. https://doi.org/10.1002/2016JD026230.
- (34) Flores, J. M.; Washenfelder, R. A.; Adler, G.; Lee, H. J.; Segev, L.; Laskin, J.; Laskin, A.; Nizkorodov, S. A.; Brown, S. S.; Rudich, Y. Complex Refractive Indices in the Near-Ultraviolet Spectral Region of Biogenic Secondary Organic Aerosol Aged with Ammonia. *Phys. Chem. Chem. Phys.* 2014, 16 (22), 10629–10642. https://doi.org/10.1039/C4CP01009D.
- (35) Li, C.; He, Q.; Hettiyadura, A. P. S.; Käfer, U.; Shmul, G.; Meidan, D.; Zimmermann, R.; Brown, S. S.; George, C.; Laskin, A.; Rudich, Y. Formation of Secondary Brown Carbon in Biomass Burning Aerosol Proxies through NO<sub>3</sub> Radical Reactions. *Environ. Sci. Technol.* **2020**, *54* (3), 1395–1405. https://doi.org/10.1021/acs.est.9b05641.
- (36) Li, C.; He, Q.; Schade, J.; Passig, J.; Zimmermann, R.; Meidan, D.; Laskin, A.; Rudich, Y. Dynamic Changes in Optical and Chemical Properties of Tar Ball Aerosols by Atmospheric Photochemical Aging. *Atmos. Chem. Phys.* **2019**, *19* (1), 139–163. https://doi.org/10.5194/acp-19-139-2019.
- (37) Lin, P.; Bluvshtein, N.; Rudich, Y.; Nizkorodov, S. A.; Laskin, J.; Laskin, A. Molecular Chemistry of Atmospheric Brown Carbon Inferred from a Nationwide Biomass Burning Event. *Environ. Sci. Technol.* 2017, 51 (20), 11561–11570. https://doi.org/10.1021/acs.est.7b02276.
- (38) Xu, J.; Hettiyadura, A. P. S.; Liu, Y.; Zhang, X.; Kang, S.; Laskin, A. Regional Differences of Chemical Composition and Optical Properties of Aerosols in the Tibetan Plateau. *JGR Atmospheres* **2020**, *125* (1), e2019JD031226. https://doi.org/10.1029/2019JD031226.
- (39) Fleming, L. T.; Lin, P.; Roberts, J. M.; Selimovic, V.; Yokelson, R.; Laskin, J.; Laskin, A.; Nizkorodov, S. A. Molecular Composition and Photochemical Lifetimes of Brown Carbon Chromophores in Biomass Burning Organic Aerosol. *Atmos. Chem. Phys.* **2020**, *20* (2), 1105–1129. https://doi.org/10.5194/acp-20-1105-2020.
- (40) Lin, P.; Fleming, L. T.; Nizkorodov, S. A.; Laskin, J.; Laskin, A. Comprehensive Molecular Characterization of Atmospheric Brown Carbon by High Resolution Mass Spectrometry with Electrospray and Atmospheric Pressure Photoionization. *Anal. Chem.* **2018**, *90* (21), 12493–12502. https://doi.org/10.1021/acs.analchem.8b02177.
- (41) Veghte, D. P.; China, S.; Weis, J.; Kovarik, L.; Gilles, M. K.; Laskin, A. Optical Properties of Airborne Soil Organic Particles. *ACS Earth Space Chem.* **2017**, *1* (8), 511–521. https://doi.org/10.1021/acsearthspacechem.7b00071.
- (42) Lin, P.; Aiona, P. K.; Li, Y.; Shiraiwa, M.; Laskin, J.; Nizkorodov, S. A.; Laskin, A. Molecular Characterization of Brown Carbon in Biomass Burning Aerosol Particles. *Environ. Sci. Technol.* **2016**, *50* (21), 11815–11824. https://doi.org/10.1021/acs.est.6b03024.
- (43) He, Q.; Bluvshtein, N.; Segev, L.; Meidan, D.; Flores, J. M.; Brown, S. S.; Brune, W.; Rudich, Y. Evolution of the Complex Refractive Index of Secondary Organic Aerosols during

- Atmospheric Aging. *Environ. Sci. Technol.* **2018**, *52* (6), 3456–3465. https://doi.org/10.1021/acs.est.7b05742.
- (44) Flores, J. M.; Zhao, D. F.; Segev, L.; Schlag, P.; Kiendler-Scharr, A.; Fuchs, H.; Watne, Å. K.; Bluvshtein, N.; Mentel, Th. F.; Hallquist, M.; Rudich, Y. Evolution of the Complex Refractive Index in the UV Spectral Region in Ageing Secondary Organic Aerosol. *Atmos. Chem. Phys.* **2014**, *14* (11), 5793–5806. https://doi.org/10.5194/acp-14-5793-2014.
- (45) West, C. P.; Hettiyadura, A. P. S.; Darmody, A.; Mahamuni, G.; Davis, J.; Novosselov, I.; Laskin, A. Molecular Composition and the Optical Properties of Brown Carbon Generated by the Ethane Flame. *ACS Earth Space Chem.* **2020**, *4* (7), 1090–1103. https://doi.org/10.1021/acsearthspacechem.0c00095.
- (46) Lambe, A. T.; Cappa, C. D.; Massoli, P.; Onasch, T. B.; Forestieri, S. D.; Martin, A. T.; Cummings, M. J.; Croasdale, D. R.; Brune, W. H.; Worsnop, D. R.; Davidovits, P. Relationship between Oxidation Level and Optical Properties of Secondary Organic Aerosol. *Environ. Sci. Technol.* **2013**, *47* (12), 6349–6357. https://doi.org/10.1021/es401043j.
- (47) Updyke, K. M.; Nguyen, T. B.; Nizkorodov, S. A. Formation of Brown Carbon via Reactions of Ammonia with Secondary Organic Aerosols from Biogenic and Anthropogenic Precursors. *Atmospheric Environment* **2012**, *63*, 22–31. https://doi.org/10.1016/j.atmosenv.2012.09.012.
- (48) Liu, P. F.; Abdelmalki, N.; Hung, H.-M.; Wang, Y.; Brune, W. H.; Martin, S. T. Ultraviolet and Visible Complex Refractive Indices of Secondary Organic Material Produced by Photooxidation of the Aromatic Compounds Toluene and M-Xylene. *Atmos. Chem. Phys.* **2015**, *15* (3), 1435–1446. https://doi.org/10.5194/acp-15-1435-2015.
- (49) Browne, E. C.; Zhang, X.; Franklin, J. P.; Ridley, K. J.; Kirchstetter, T. W.; Wilson, K. R.; Cappa, C. D.; Kroll, J. H. Effect of Heterogeneous Oxidative Aging on Light Absorption by Biomass Burning Organic Aerosol. *Aerosol Science and Technology* **2019**, *53* (6), 663–674. https://doi.org/10.1080/02786826.2019.1599321.
- (50) Sengupta, D.; Samburova, V.; Bhattarai, C.; Kirillova, E.; Mazzoleni, L.; Iaukea-Lum, M.; Watts, A.; Moosmüller, H.; Khlystov, A. Light Absorption by Polar and Non-Polar Aerosol Compounds from Laboratory Biomass Combustion. *Atmos. Chem. Phys.* **2018**, *18* (15), 10849–10867. https://doi.org/10.5194/acp-18-10849-2018.
- (51) Xie, M.; Shen, G.; Holder, A. L.; Hays, M. D.; Jetter, J. J. Light Absorption of Organic Carbon Emitted from Burning Wood, Charcoal, and Kerosene in Household Cookstoves. *Environmental Pollution* **2018**, *240*, 60–67. https://doi.org/10.1016/j.envpol.2018.04.085.
- (52) Huang, R.-J.; Yang, L.; Cao, J.; Chen, Y.; Chen, Q.; Li, Y.; Duan, J.; Zhu, C.; Dai, W.; Wang, K.; Lin, C.; Ni, H.; Corbin, J. C.; Wu, Y.; Zhang, R.; Tie, X.; Hoffmann, T.; O'Dowd, C.; Dusek, U. Brown Carbon Aerosol in Urban Xi'an, Northwest China: The Composition and Light Absorption Properties. *Environ. Sci. Technol.* 2018, 52 (12), 6825–6833. https://doi.org/10.1021/acs.est.8b02386.
- (53) Yuan, W.; Huang, R.-J.; Yang, L.; Guo, J.; Chen, Z.; Duan, J.; Wang, T.; Ni, H.; Han, Y.; Li, Y.; Chen, Q.; Chen, Y.; Hoffmann, T.; O'Dowd, C. Characterization of the Light-Absorbing Properties, Chromophore Composition and Sources of Brown Carbon Aerosol in Xi'an, Northwestern China. *Atmos. Chem. Phys.* **2020**, *20* (8), 5129–5144. https://doi.org/10.5194/acp-20-5129-2020.
- (54) Hems, R. F.; Abbatt, J. P. D. Aqueous Phase Photo-Oxidation of Brown Carbon Nitrophenols: Reaction Kinetics, Mechanism, and Evolution of Light Absorption. *ACS Earth Space Chem.* **2018**, *2* (3), 225–234. https://doi.org/10.1021/acsearthspacechem.7b00123.

- (55) Trofimova, A.; Hems, R. F.; Liu, T.; Abbatt, J. P. D.; Schnitzler, E. G. Contribution of Charge-Transfer Complexes to Absorptivity of Primary Brown Carbon Aerosol. *ACS Earth Space Chem.* **2019**, *3* (8), 1393–1401. https://doi.org/10.1021/acsearthspacechem.9b00116.
- (56) Di Lorenzo, R. A.; Washenfelder, R. A.; Attwood, A. R.; Guo, H.; Xu, L.; Ng, N. L.; Weber, R. J.; Baumann, K.; Edgerton, E.; Young, C. J. Molecular-Size-Separated Brown Carbon Absorption for Biomass-Burning Aerosol at Multiple Field Sites. *Environ. Sci. Technol.* **2017**, *51* (6), 3128–3137. https://doi.org/10.1021/acs.est.6b06160.
- (57) Saleh, R.; Hennigan, C. J.; McMeeking, G. R.; Chuang, W. K.; Robinson, E. S.; Coe, H.; Donahue, N. M.; Robinson, A. L. Absorptivity of Brown Carbon in Fresh and Photo-Chemically Aged Biomass-Burning Emissions. *Atmos. Chem. Phys.* **2013**, *13* (15), 7683–7693. https://doi.org/10.5194/acp-13-7683-2013.
- (58) Kumar, N. K.; Corbin, J. C.; Bruns, E. A.; Massabó, D.; Slowik, J. G.; Drinovec, L.; Močnik, G.; Prati, P.; Vlachou, A.; Baltensperger, U.; Gysel, M.; El-Haddad, I.; Prévôt, A. S. H. Production of Particulate Brown Carbon during Atmospheric Aging of Residential Wood-Burning Emissions. *Atmos. Chem. Phys.* 2018, 18 (24), 17843–17861. https://doi.org/10.5194/acp-18-17843-2018.
- (59) Saleh, R. From Measurements to Models: Toward Accurate Representation of Brown Carbon in Climate Calculations. *Curr Pollution Rep* **2020**, *6* (2), 90–104. https://doi.org/10.1007/s40726-020-00139-3.
- (60) Siemens, K.; Morales, A.; He, Q.; Li, C.; Hettiyadura, A. P. S.; Rudich, Y.; Laskin, A. Molecular Analysis of Secondary Brown Carbon Produced from the Photooxidation of Naphthalene. *Environ. Sci. Technol.* 2022, 56 (6), 3340–3353. https://doi.org/10.1021/acs.est.1c03135.
- (61) Klodt, A. L.; Aiona, P. K.; MacMillan, A. C.; Ji (Julie) Lee, H.; Zhang, X.; Helgestad, T.; Novak, G. A.; Lin, P.; Laskin, J.; Laskin, A.; Bertram, T. H.; Cappa, C. D.; Nizkorodov, S. A. Effect of Relative Humidity, NO<sub>x</sub>, and Ammonia on the Physical Properties of Naphthalene Secondary Organic Aerosols. *Environ. Sci.: Atmos.* **2023**, *3* (6), 991–1007. https://doi.org/10.1039/D3EA00033H.
- (62) Hettiyadura, A. P. S.; Garcia, V.; Li, C.; West, C. P.; Tomlin, J.; He, Q.; Rudich, Y.; Laskin, A. Chemical Composition and Molecular-Specific Optical Properties of Atmospheric Brown Carbon Associated with Biomass Burning. *Environ. Sci. Technol.* **2021**, *55* (4), 2511–2521. https://doi.org/10.1021/acs.est.0c05883.
- (63) Jiang, W.; Ma, L.; Niedek, C.; Anastasio, C.; Zhang, Q. Chemical and Light-Absorption Properties of Water-Soluble Organic Aerosols in Northern California and Photooxidant Production by Brown Carbon Components. *ACS Earth Space Chem.* **2023**, *7* (5), 1107–1119. https://doi.org/10.1021/acsearthspacechem.3c00022.
- (64) Baboomian, V. J.; He, Q.; Montoya-Aguilera, J.; Ali, N.; Fleming, L. T.; Lin, P.; Laskin, A.; Laskin, J.; Rudich, Y.; Nizkorodov, S. A. Light Absorption and Scattering Properties of Indole Secondary Organic Aerosol Prepared under Various Oxidant and Relative Humidity Conditions. *Aerosol Science and Technology* 2023, 57 (6), 532–545. https://doi.org/10.1080/02786826.2023.2193235.
- (65) Kirchstetter, T. W.; Novakov, T.; Hobbs, P. V. Evidence That the Spectral Dependence of Light Absorption by Aerosols Is Affected by Organic Carbon. J. Geophys. Res. 2004, 109 (D21), D21208. https://doi.org/10.1029/2004JD004999.

- (66) Alexander, D. T. L.; Crozier, P. A.; Anderson, J. R. Brown Carbon Spheres in East Asian Outflow and Their Optical Properties. *Science* **2008**, *321* (5890), 833–836. https://doi.org/10.1126/science.1155296.
- (67) Laskin, J.; Laskin, A.; Nizkorodov, S. A. Mass Spectrometry Analysis in Atmospheric Chemistry. *Anal. Chem.* **2018**, 90 (1), 166–189. https://doi.org/10.1021/acs.analchem.7b04249.
- (68) Jiang, H.-X.; Li, J.; Tang, J.; Mo, Y.-Z.; Zhang, G. Applications of High-Resolution Mass Spectrometry in Studies of Brown Carbon. *Chinese Journal of Analytical Chemistry* **2018**, *46* (10), 1528–1538. https://doi.org/10.1016/S1872-2040(18)61115-6.
- (69) Di Lorenzo, R. A.; Young, C. J. Size Separation Method for Absorption Characterization in Brown Carbon: Application to an Aged Biomass Burning Sample. *Geophysical Research Letters* **2016**, *43* (1), 458–465. https://doi.org/10.1002/2015GL066954.
- (70) Baboomian, V. J.; Gu, Y.; Nizkorodov, S. A. Photodegradation of Secondary Organic Aerosols by Long-Term Exposure to Solar Actinic Radiation. *ACS Earth Space Chem.* **2020**, 4 (7), 1078–1089. https://doi.org/10.1021/acsearthspacechem.0c00088.
- (71) Fang, Z.; Li, C.; He, Q.; Czech, H.; Gröger, T.; Zeng, J.; Fang, H.; Xiao, S.; Pardo, M.; Hartner, E.; Meidan, D.; Wang, X.; Zimmermann, R.; Laskin, A.; Rudich, Y. Secondary Organic Aerosols Produced from Photochemical Oxidation of Secondarily Evaporated Biomass Burning Organic Gases: Chemical Composition, Toxicity, Optical Properties, and Climate Effect. *Environment International* **2021**, *157*, 106801. https://doi.org/10.1016/j.envint.2021.106801.
- (72) Loebel Roson, M.; Abou-Ghanem, M.; Kim, E.; Wu, S.; Long, D.; Styler, S. A.; Zhao, R. Unexpected Electrophiles in the Atmosphere Anhydride Nucleophile Reactions and Uptake to Biomass Burning Emissions. *Phys. Chem. Chem. Phys.* **2023**, *25* (28), 18742–18756. https://doi.org/10.1039/D3CP01751F.
- (73) Al-Mashala, H. H.; Betz, K. L.; Calvert, C. T.; Barton, J. A.; Bruce, E. E.; Schnitzler, E. G. Ultraviolet Irradiation Can Increase the Light Absorption and Viscosity of Primary Brown Carbon from Biomass Burning. *ACS Earth Space Chem.* **2023**, 7 (10), 1882–1889. https://doi.org/10.1021/acsearthspacechem.3c00155.
- (74) Laskin, J.; Laskin, A.; Nizkorodov, S. A.; Roach, P.; Eckert, P.; Gilles, M. K.; Wang, B.; Lee, H. J. (Julie); Hu, Q. Molecular Selectivity of Brown Carbon Chromophores. *Environ. Sci. Technol.* **2014**, *48* (20), 12047–12055. https://doi.org/10.1021/es503432r.
- (75) Liu, F.; Yon, J.; Fuentes, A.; Lobo, P.; Smallwood, G. J.; Corbin, J. C. Review of Recent Literature on the Light Absorption Properties of Black Carbon: Refractive Index, Mass Absorption Cross Section, and Absorption Function. *Aerosol Science and Technology* **2020**, 54 (1), 33–51. https://doi.org/10.1080/02786826.2019.1676878.
- (76) Xu, J.; Hettiyadura, A. P. S.; Liu, Y.; Zhang, X.; Kang, S.; Laskin, A. Atmospheric Brown Carbon on the Tibetan Plateau: Regional Differences in Chemical Composition and Light Absorption Properties. *Environ. Sci. Technol. Lett.* **2022**, *9* (3), 219–225. https://doi.org/10.1021/acs.estlett.2c00016.
- (77) Huang, R.-J.; Yang, L.; Shen, J.; Yuan, W.; Gong, Y.; Ni, H.; Duan, J.; Yan, J.; Huang, H.; You, Q.; Li, Y. J. Chromophoric Fingerprinting of Brown Carbon from Residential Biomass Burning. *Environ. Sci. Technol. Lett.* **2022**, *9* (2), 102–111. https://doi.org/10.1021/acs.estlett.1c00837.
- (78) Misovich, M. V.; Hettiyadura, A. P. S.; Jiang, W.; Zhang, Q.; Laskin, A. Molecular-Level Study of the Photo-Oxidation of Aqueous-Phase Guaiacyl Acetone in the Presence of <sup>3</sup>C\*:

- Formation of Brown Carbon Products. *ACS Earth Space Chem.* **2021**, *5* (8), 1983–1996. https://doi.org/10.1021/acsearthspacechem.1c00103.
- (79) Rodriguez, A. A.; Rafla, M. A.; Welsh, H. G.; Pennington, E. A.; Casar, J. R.; Hawkins, L. N.; Jimenez, N. G.; De Loera, A.; Stewart, D. R.; Rojas, A.; Tran, M.-K.; Lin, P.; Laskin, A.; Formenti, P.; Cazaunau, M.; Pangui, E.; Doussin, J.-F.; De Haan, D. O. Kinetics, Products, and Brown Carbon Formation by Aqueous-Phase Reactions of Glycolaldehyde with Atmospheric Amines and Ammonium Sulfate. *J. Phys. Chem. A* **2022**, *126* (32), 5375–5385. https://doi.org/10.1021/acs.jpca.2c02606.
- (80) Lavi, A.; Lin, P.; Bhaduri, B.; Carmieli, R.; Laskin, A.; Rudich, Y. Characterization of Light-Absorbing Oligomers from Reactions of Phenolic Compounds and Fe(III). *ACS Earth Space Chem.* **2017**, *I* (10), 637–646. https://doi.org/10.1021/acsearthspacechem.7b00099.
- (81) Zhang, X.; Lin, Y.-H.; Surratt, J. D.; Weber, R. J. Sources, Composition and Absorption Angström Exponent of Light-Absorbing Organic Components in Aerosol Extracts from the Los Angeles Basin. *Environ. Sci. Technol.* **2013**, *47* (8), 3685–3693. https://doi.org/10.1021/es305047b.
- (82) Budisulistiorini, S. H.; Riva, M.; Williams, M.; Chen, J.; Itoh, M.; Surratt, J. D.; Kuwata, M. Light-Absorbing Brown Carbon Aerosol Constituents from Combustion of Indonesian Peat and Biomass. *Environ. Sci. Technol.* 2017, 51 (8), 4415–4423. https://doi.org/10.1021/acs.est.7b00397.
- (83) Bai, Z.; Zhang, L.; Cheng, Y.; Zhang, W.; Mao, J.; Chen, H.; Li, L.; Wang, L.; Chen, J. Water/Methanol-Insoluble Brown Carbon Can Dominate Aerosol-Enhanced Light Absorption in Port Cities. *Environ. Sci. Technol.* **2020**, *54* (23), 14889–14898. https://doi.org/10.1021/acs.est.0c03844.
- (84) Jiang, X.; Liu, D.; Li, Q.; Tian, P.; Wu, Y.; Li, S.; Hu, K.; Ding, S.; Bi, K.; Li, R.; Huang, M.; Ding, D.; Chen, Q.; Kong, S.; Li, W.; Pang, Y.; He, D. Connecting the Light Absorption of Atmospheric Organic Aerosols with Oxidation State and Polarity. *Environ. Sci. Technol.* 2022, 56 (18), 12873–12885. https://doi.org/10.1021/acs.est.2c02202.
- (85) Mie, G. Beiträge zur Optik trüber Medien, speziell kolloidaler Metallösungen. *Ann. Phys.* **1908**, *330* (3), 377–445. https://doi.org/10.1002/andp.19083300302.
- (86) He, Q.; Li, C.; Siemens, K.; Morales, A. C.; Hettiyadura, A. P. S.; Laskin, A.; Rudich, Y. Optical Properties of Secondary Organic Aerosol Produced by Photooxidation of Naphthalene under NOx Condition. *Environ. Sci. Technol.* 2022, 56 (8), 4816–4827. https://doi.org/10.1021/acs.est.1c07328.
- (87) Li, C.; He, Q.; Fang, Z.; Brown, S. S.; Laskin, A.; Cohen, S. R.; Rudich, Y. Laboratory Insights into the Diel Cycle of Optical and Chemical Transformations of Biomass Burning Brown Carbon Aerosols. *Environ. Sci. Technol.* **2020**, *54* (19), 11827–11837. https://doi.org/10.1021/acs.est.0c04310.
- (88) He, Q.; Tomaz, S.; Li, C.; Zhu, M.; Meidan, D.; Riva, M.; Laskin, A.; Brown, S. S.; George, C.; Wang, X.; Rudich, Y. Optical Properties of Secondary Organic Aerosol Produced by Nitrate Radical Oxidation of Biogenic Volatile Organic Compounds. *Environ. Sci. Technol.* **2021**, *55* (5), 2878–2889. https://doi.org/10.1021/acs.est.0c06838.
- (89) Ohlemiller, T. J. Modeling of Smoldering Combustion Propagation. *Progress in Energy and Combustion Science* **1985**, *11* (4), 277–310. https://doi.org/10.1016/0360-1285(85)90004-8
- (90) Mohan, D.; Pittman, C. U.; Steele, P. H. Pyrolysis of Wood/Biomass for Bio-Oil: A Critical Review. *Energy Fuels* **2006**, *20* (3), 848–889. https://doi.org/10.1021/ef0502397.

- (91) Tóth, A.; Hoffer, A.; Nyirő-Kósa, I.; Pósfai, M.; Gelencsér, A. Atmospheric Tar Balls: Aged Primary Droplets from Biomass Burning? *Atmos. Chem. Phys.* **2014**, *14* (13), 6669–6675. https://doi.org/10.5194/acp-14-6669-2014.
- (92) Bateman, A. P.; Walser, M. L.; Desyaterik, Y.; Laskin, J.; Laskin, A.; Nizkorodov, S. A. The Effect of Solvent on the Analysis of Secondary Organic Aerosol Using Electrospray Ionization Mass Spectrometry. *Environ. Sci. Technol.* **2008**, *42* (19), 7341–7346. https://doi.org/10.1021/es801226w.
- (93) Chen, K.; Raeofy, N.; Lum, M.; Mayorga, R.; Woods, M.; Bahreini, R.; Zhang, H.; Lin, Y.-H. Solvent Effects on Chemical Composition and Optical Properties of Extracted Secondary Brown Carbon Constituents. *Aerosol Science and Technology* **2022**, *56* (10), 917–930. https://doi.org/10.1080/02786826.2022.2100734.
- (94) Siemens, K. S. A.; Pagonis, D.; Guo, H.; Schueneman, M. K.; Dibb, J. E.; Campuzano-Jost, P.; Jimenez, J. L.; Laskin, A. Probing Atmospheric Aerosols by Multimodal Mass Spectrometry Techniques: Revealing Aging Characteristics of Its Individual Molecular Components. *ACS Earth Space Chem.* **2023**, 7 (12), 2498–2510. https://doi.org/10.1021/acsearthspacechem.3c00228.
- (95) Chen, Y.; Bond, T. C. Light Absorption by Organic Carbon from Wood Combustion. *Atmos. Chem. Phys.* **2010**, *10* (4), 1773–1787. https://doi.org/10.5194/acp-10-1773-2010.
- (96) Smith, D. R.; Robb, D. B.; Blades, M. W. Comparison of Dopants for Charge Exchange Ionization of Nonpolar Polycyclic Aromatic Hydrocarbons with Reversed-Phase LC-APPI-MS. J. Am. Soc. Mass Spectrom. 2009, 20 (1), 73–79. https://doi.org/10.1016/j.jasms.2008.09.012.
- (97) Cai, S.-S.; Syage, J. A.; Hanold, K. A.; Balogh, M. P. Ultra Performance Liquid Chromatography—Atmospheric Pressure Photoionization-Tandem Mass Spectrometry for High-Sensitivity and High-Throughput Analysis of U.S. Environmental Protection Agency 16 Priority Pollutants Polynuclear Aromatic Hydrocarbons. *Anal. Chem.* **2009**, *81* (6), 2123–2128. https://doi.org/10.1021/ac802275e.
- (98) Pelillo, M.; Cuvelier, M. E.; Biguzzi, B.; Gallina Toschi, T.; Berset, C.; Lercker, G. Calculation of the Molar Absorptivity of Polyphenols by Using Liquid Chromatography with Diode Array Detection: The Case of Carnosic Acid. *Journal of Chromatography A* **2004**, *1023* (2), 225–229. https://doi.org/10.1016/S0021-9673(03)01206-8.
- (99) Hettiyadura, A. P. S.; Laskin, A. Quantitative Analysis of Polycyclic Aromatic Hydrocarbons Using High-performance Liquid Chromatography-photodiode Array-high-resolution Mass Spectrometric Detection Platform Coupled to Electrospray and Atmospheric Pressure Photoionization Sources. *J Mass Spectrom* **2022**, *57* (2), e4804. https://doi.org/10.1002/jms.4804.
- (100) Schmid, R.; Heuckeroth, S.; Korf, A.; Smirnov, A.; Myers, O.; Dyrlund, T. S.; Bushuiev, R.; Murray, K. J.; Hoffmann, N.; Lu, M.; Sarvepalli, A.; Zhang, Z.; Fleischauer, M.; Dührkop, K.; Wesner, M.; Hoogstra, S. J.; Rudt, E.; Mokshyna, O.; Brungs, C.; Ponomarov, K.; Mutabdžija, L.; Damiani, T.; Pudney, C. J.; Earll, M.; Helmer, P. O.; Fallon, T. R.; Schulze, T.; Rivas-Ubach, A.; Bilbao, A.; Richter, H.; Nothias, L.-F.; Wang, M.; Orešič, M.; Weng, J.-K.; Böcker, S.; Jeibmann, A.; Hayen, H.; Karst, U.; Dorrestein, P. C.; Petras, D.; Du, X.; Pluskal, T. Integrative Analysis of Multimodal Mass Spectrometry Data in MZmine 3. *Nat Biotechnol* 2023, *41* (4), 447–449. https://doi.org/10.1038/s41587-023-01690-2.

- (101) Roach, P. J.; Laskin, J.; Laskin, A. Higher-Order Mass Defect Analysis for Mass Spectra of Complex Organic Mixtures. *Anal. Chem.* **2011**, *83* (12), 4924–4929. https://doi.org/10.1021/ac200654j.
- (102) McLafferty, F. W.; Tureček, F. *Interpretation of Mass Spectra*, 4th ed.; University Science Books: Mill Valley, Calif, 1993.
- (103) Krevelen, V. Graphical-Statistical Method for the Study of Structure and Reaction Processes of Coal. *Fuel* **1950**, *29*, 269–284.
- (104) Zhang, Y.; Wang, K.; Tong, H.; Huang, R.; Hoffmann, T. The Maximum Carbonyl Ratio (MCR) as a New Index for the Structural Classification of Secondary Organic Aerosol Components. *Rapid Commun Mass Spectrom* **2021**, *35* (14). https://doi.org/10.1002/rcm.9113.
- (105) Kroll, J. H.; Lim, C. Y.; Kessler, S. H.; Wilson, K. R. Heterogeneous Oxidation of Atmospheric Organic Aerosol: Kinetics of Changes to the Amount and Oxidation State of Particle-Phase Organic Carbon. *J. Phys. Chem. A* **2015**, *119* (44), 10767–10783. https://doi.org/10.1021/acs.jpca.5b06946.
- (106) Li, Y.; Pöschl, U.; Shiraiwa, M. Molecular Corridors and Parameterizations of Volatility in the Chemical Evolution of Organic Aerosols. *Atmos. Chem. Phys.* **2016**, *16* (5), 3327–3344. https://doi.org/10.5194/acp-16-3327-2016.
- (107) Angell, C. A. Relaxation in Liquids, Polymers and Plastic Crystals Strong/Fragile Patterns and Problems. *Journal of Non-Crystalline Solids* **1991**, *131–133*, 13–31. https://doi.org/10.1016/0022-3093(91)90266-9.
- (108) DeRieux, W.-S. W.; Li, Y.; Lin, P.; Laskin, J.; Laskin, A.; Bertram, A. K.; Nizkorodov, S. A.; Shiraiwa, M. Predicting the Glass Transition Temperature and Viscosity of Secondary Organic Material Using Molecular Composition. *Atmos. Chem. Phys.* **2018**, *18* (9), 6331–6351. https://doi.org/10.5194/acp-18-6331-2018.
- (109) Li, Y.; Day, D. A.; Stark, H.; Jimenez, J. L.; Shiraiwa, M. Predictions of the Glass Transition Temperature and Viscosity of Organic Aerosols from Volatility Distributions. *Atmos. Chem. Phys.* **2020**, *20* (13), 8103–8122. https://doi.org/10.5194/acp-20-8103-2020.
- (110) Hoffer, A.; Tóth, A.; Nyirő-Kósa, I.; Pósfai, M.; Gelencsér, A. Light Absorption Properties of Laboratory-Generated Tar Ball Particles. *Atmos. Chem. Phys.* **2016**, *16* (1), 239–246. https://doi.org/10.5194/acp-16-239-2016.
- (111) Jones, S. H.; Friederich, P.; Donaldson, D. J. Photochemical Aging of Levitated Aqueous Brown Carbon Droplets. *ACS Earth Space Chem.* **2021**, *5* (4), 749–754. https://doi.org/10.1021/acsearthspacechem.1c00005.
- (112) Sedlacek III, A. J.; Buseck, P. R.; Adachi, K.; Onasch, T. B.; Springston, S. R.; Kleinman, L. Formation and Evolution of Tar Balls from Northwestern US Wildfires. *Atmos. Chem. Phys.* **2018**, *18* (15), 11289–11301. https://doi.org/10.5194/acp-18-11289-2018.
- (113) Adachi, K.; Sedlacek, A. J.; Kleinman, L.; Springston, S. R.; Wang, J.; Chand, D.; Hubbe, J. M.; Shilling, J. E.; Onasch, T. B.; Kinase, T.; Sakata, K.; Takahashi, Y.; Buseck, P. R. Spherical Tarball Particles Form through Rapid Chemical and Physical Changes of Organic Matter in Biomass-Burning Smoke. *Proc. Natl. Acad. Sci. U.S.A.* **2019**, *116* (39), 19336–19341. https://doi.org/10.1073/pnas.1900129116.
- (114) Adachi, K.; Buseck, P. R. Atmospheric Tar Balls from Biomass Burning in Mexico. *J. Geophys. Res.* **2011**, *116* (D5), D05204. https://doi.org/10.1029/2010JD015102.
- (115) Pagonis, D.; Selimovic, V.; Campuzano-Jost, P.; Guo, H.; Day, D. A.; Schueneman, M. K.; Nault, B. A.; Coggon, M. M.; DiGangi, J. P.; Diskin, G. S.; Fortner, E. C.; Gargulinski, E. M.; Gkatzelis, G. I.; Hair, J. W.; Herndon, S. C.; Holmes, C. D.; Katich, J. M.; Nowak, J. B.;

- Perring, A. E.; Saide, P.; Shingler, T. J.; Soja, A. J.; Thapa, L. H.; Warneke, C.; Wiggins, E. B.; Wisthaler, A.; Yacovitch, T. I.; Yokelson, R. J.; Jimenez, J. L. Impact of Biomass Burning Organic Aerosol Volatility on Smoke Concentrations Downwind of Fires. *Environ. Sci. Technol.* **2023**, *57* (44), 17011–17021. https://doi.org/10.1021/acs.est.3c05017.
- (116) Mathai, S.; Veghte, D.; Kovarik, L.; Mazzoleni, C.; Tseng, K.-P.; Bucci, S.; Capek, T.; Cheng, Z.; Marinoni, A.; China, S. Optical Properties of Individual Tar Balls in the Free Troposphere. *Environ. Sci. Technol.* **2023**, *57* (44), 16834–16842. https://doi.org/10.1021/acs.est.3c03498.
- (117) Marshall, F. H.; Miles, R. E. H.; Song, Y.-C.; Ohm, P. B.; Power, R. M.; Reid, J. P.; Dutcher, C. S. Diffusion and Reactivity in Ultraviscous Aerosol and the Correlation with Particle Viscosity. *Chem. Sci.* **2016**, *7* (2), 1298–1308. https://doi.org/10.1039/C5SC03223G.
- (118) Shiraiwa, M.; Ammann, M.; Koop, T.; Pöschl, U. Gas Uptake and Chemical Aging of Semisolid Organic Aerosol Particles. *Proc. Natl. Acad. Sci. U.S.A.* **2011**, *108* (27), 11003–11008. https://doi.org/10.1073/pnas.1103045108.
- (119) Berkemeier, T.; Steimer, S. S.; Krieger, U. K.; Peter, T.; Pöschl, U.; Ammann, M.; Shiraiwa, M. Ozone Uptake on Glassy, Semi-Solid and Liquid Organic Matter and the Role of Reactive Oxygen Intermediates in Atmospheric Aerosol Chemistry. *Phys. Chem. Chem. Phys.* **2016**, *18* (18), 12662–12674. https://doi.org/10.1039/C6CP00634E.
- (120) Wang, B.; O'Brien, R. E.; Kelly, S. T.; Shilling, J. E.; Moffet, R. C.; Gilles, M. K.; Laskin, A. Reactivity of Liquid and Semisolid Secondary Organic Carbon with Chloride and Nitrate in Atmospheric Aerosols. *J. Phys. Chem. A* **2015**, *119* (19), 4498–4508. https://doi.org/10.1021/jp510336q.
- (121) Wong, J. P. S.; Zhou, S.; Abbatt, J. P. D. Changes in Secondary Organic Aerosol Composition and Mass Due to Photolysis: Relative Humidity Dependence. *J. Phys. Chem. A* **2015**, *119* (19), 4309–4316. https://doi.org/10.1021/jp506898c.
- (122) Lignell, H.; Hinks, M. L.; Nizkorodov, S. A. Exploring Matrix Effects on Photochemistry of Organic Aerosols. *Proc. Natl. Acad. Sci. U.S.A.* **2014**, *111* (38), 13780–13785. https://doi.org/10.1073/pnas.1322106111.
- (123) Reid, J. P.; Bertram, A. K.; Topping, D. O.; Laskin, A.; Martin, S. T.; Petters, M. D.; Pope, F. D.; Rovelli, G. The Viscosity of Atmospherically Relevant Organic Particles. *Nat Commun* **2018**, *9* (1), 956. https://doi.org/10.1038/s41467-018-03027-z.
- (124) Koop, T.; Bookhold, J.; Shiraiwa, M.; Pöschl, U. Glass Transition and Phase State of Organic Compounds: Dependency on Molecular Properties and Implications for Secondary Organic Aerosols in the Atmosphere. *Phys. Chem. Chem. Phys.* **2011**, *13* (43), 19238. https://doi.org/10.1039/c1cp22617g.
- (125) Chakrabarty, R. K.; Shetty, N. J.; Thind, A. S.; Beeler, P.; Sumlin, B. J.; Zhang, C.; Liu, P.; Idrobo, J. C.; Adachi, K.; Wagner, N. L.; Schwarz, J. P.; Ahern, A.; Sedlacek, A. J.; Lambe, A.; Daube, C.; Lyu, M.; Liu, C.; Herndon, S.; Onasch, T. B.; Mishra, R. Shortwave Absorption by Wildfire Smoke Dominated by Dark Brown Carbon. *Nat. Geosci.* **2023**, *16* (8), 683–688. https://doi.org/10.1038/s41561-023-01237-9.
- (126) Zhu, J.; Crozier, P. A.; Ercius, P.; Anderson, J. R. Derivation of Optical Properties of Carbonaceous Aerosols by Monochromated Electron Energy-Loss Spectroscopy. *Microsc Microanal* **2014**, *20* (3), 748–759. https://doi.org/10.1017/S143192761400049X.
- (127) Huang, R.-J.; Yang, L.; Shen, J.; Yuan, W.; Gong, Y.; Guo, J.; Cao, W.; Duan, J.; Ni, H.; Zhu, C.; Dai, W.; Li, Y.; Chen, Y.; Chen, Q.; Wu, Y.; Zhang, R.; Dusek, U.; O'Dowd, C.; Hoffmann, T. Water-Insoluble Organics Dominate Brown Carbon in Wintertime Urban

- Aerosol of China: Chemical Characteristics and Optical Properties. *Environ. Sci. Technol.* **2020**, *54* (13), 7836–7847. https://doi.org/10.1021/acs.est.0c01149.
- (128) Shiraiwa, M.; Li, Y.; Tsimpidi, A. P.; Karydis, V. A.; Berkemeier, T.; Pandis, S. N.; Lelieveld, J.; Koop, T.; Pöschl, U. Global Distribution of Particle Phase State in Atmospheric Secondary Organic Aerosols. *Nat Commun* **2017**, 8 (1), 15002. https://doi.org/10.1038/ncomms15002.